FEATURE ARTICLE

Describing the Diffusion of Guest Molecules Inside Porous Structures

Rajamani Krishna*

Van't Hoff Institute for Molecular Sciences, University of Amsterdam, Nieuwe Achtergracht 166, 1018 WV Amsterdam, The Netherlands

Received: July 21, 2009; Revised Manuscript Received: August 22, 2009

The design and development of many emerging separation and catalytic process technologies require a proper quantitative description of diffusion of mixtures of guest molecules within meso- and microporous structures. In mesoporous materials with pore sizes 2 nm $< d_p <$ 50 nm, there is a central core region where the influence of interactions of the molecules with the pore wall is either small or negligible; mesopore diffusion is governed by a combination of molecule−molecule and molecule−pore wall interactions. Within micropores with $d_p <$ 2 nm, the guest molecules are always within the influence of the force field exerted with the wall; we have to reckon with the motion of adsorbed molecules, and there is no "bulk" fluid region. This article presents a unified, phenomenological, description of diffusion inside meso- and microporous structures using concepts and ideas that originate from James Clerk Maxwell and Josef Stefan. With the aid of extensive data sets of molecular dynamic simulations of unary and mixture diffusion in a wide variety of materials such as zeolites, metal-organic frameworks, covalent organic frameworks, carbon nanotubes, and cylindrical silica pores with a diverse range of pore topologies and pore sizes, we derive a molecular-level understanding of the various coefficients that arise in the phenomenological Maxwell−Stefan diffusion formulation. This understanding helps us to explain and describe a variety of experimental data and observations. We also demonstrate how a molecular level understanding aids separation and reaction process development.

1. Introduction

A wide variety of ordered porous materials are used in a range of applications in storage, separation, and catalysis.[1−8] These include microporous structures such as zeolites (crystalline aluminosilicates), carbon nanotubes (CNTs), carbon molecular sieves (CMS), metal-organic frameworks (MOFs), covalent organic frameworks (COFs), titanosilicates (such as ETS-4, and ETS-10) and mesoporous materials, such as SBA-16, MCM-41, and Vycor Glass; see Figure 1. In several applications, it is necessary to have a good understanding and description of the diffusion of guest molecules inside the porous structures. For example, the development of a membrane process for separating CO_2 from CH_4 relies on an accurate description of both adsorption and diffusion within micropores at high molecular loadings.[9] In zeolite-catalyzed alkylation, isomerization, and cracking processes, the selectivity and product slate depends on subtle diffusional effects.[10−13] The focus of this paper is on diffusion inside crystallographically well-defined porous structures with regular pore geometries and shapes; amorphous materials are not within the scope of our discussions.

The underlying theme of this article is to demonstrate that the fundamental understanding of diffusion of guest molecules in porous structures is significantly aided and enhanced with the use of molecular simulation techniques: Monte Carlo (MC) simulations of adsorption isotherms in the grand-canonical (GC) ensemble, molecular dynamics (MD) simulations of diffusivities, and transition state theory (TST) calculations of free energy profiles and barriers. Molecular simulations are shown to be potent adjuncts to experiments. Details of simulation techniques are not provided in this article; the reader is referred to published papers[12−28] and books.[29,30]

We begin with the description of diffusion of pure component species, and subsequently move on to the description of mixture transport. Throughout the discussions, our aim is to provide molecular-level interpretations of the variety of phenomenological transport coefficients.

2. Describing Unary Diffusion

Fick's law relates the flux N_i of species i to the gradient of the loading or concentration by postulating[31,32]

$$N_i = c_i u_i = -D_i \nabla c_i \tag{1}$$

In eq 1, D_i is the Fick diffusivity, and u_i is the ensemble average velocity of species i and is set up in a reference frame with respect to the host framework. The concentrations c_i are expressed as the number of moles per cubic meter of pore volume. For any porous structure, the accessible pore volumes V_{pore} can be determined experimentally or with the aid of molecular simulations using the helium probe insertion technique suggested by Talu and Myers.[33,34] For micropore diffusion, the loadings are more commonly expressed in the published literature in units such as moles per kilograms of framework (q_i), or molecules per unit cell (Θ_i). There are persuasive advantages to using the c_i for description of both micro- and mesopore diffusion;[35] these will become apparent later. We have

* To whom correspondence should be addressed. E-mail: r.krishna@uva.nl.

10.1021/jp906879d CCC: $40.75
Published on Web 09/18/2009

Rajamani Krishna received his B.S. (1968) and Ph.D. (1975) degrees in Chemical Engineering from the Universities of Bombay and Manchester, respectively. During 1970−1975, he served on the faculty of the University of Manchester, before joining the Shell group of companies in The Netherlands. During the period 1976−1984, he was involved in a wide variety of reaction and separation process developmental activities within Shell. Subsequently, he served as Director of the Indian Institute of Petroleum before taking up his current position of Professor at the University of Amsterdam in 1990. His research interests include molecular simulations of adsorption and diffusion in porous materials, multiphase reactor hydrodynamics, and reactive distillation. He has published three text books on mass transfer, has more than 300 peer-reviewed publications, and holds several patents. Currently, his *h*-index is 44.

the interrelation $c_i = q_i/V_{pore}$. A further point to note is that the flux N_i is defined in terms of the pore cross-sectional area; multiplication by the pore volume fraction is required to obtain fluxes in terms of the area of the crystalline framework.

The Fick diffusivity D_i, also referred to as the "transport" diffusivity, is determinable from say uptake or chromatographic experiments.[31,32] The D_i is strongly influenced by the adsorption equilibrium, especially in the cases of micropores, and is therefore not susceptible to simple molecular interpretation. For the purpose of theoretical understanding and modeling, it is necessary to adopt a more fundamental approach based on irreversible thermodynamics with the chemical potential gradients $\nabla\mu_i$ as driving forces. Following Onsager, we may postulate

$$N_i = -\frac{1}{RT} L_i \nabla\mu_i \tag{2}$$

where L_i is the Onsager coefficient. It is advantageous and preferable to use the alternative, but formally equivalent, Maxwell−Stefan (M-S) or "friction" formulation,[36] driving force = (drag coefficient) × (relative velocity with respective to the framework)

$$-\nabla\mu_i = \frac{RT}{Đ_i} u_i; \quad N_i = -\frac{1}{RT} Đ_i c_i \nabla\mu_i \tag{3}$$

The $Đ_i$ is the M-S diffusivity; this reflects molecule-wall interaction processes in a general sense. The term $(RT/Đ_i)$ in eq 3 may be interpreted as the drag coefficient between the molecules and the pore wall.[36]

The $\nabla\mu_i$ are related to the ∇c_i by introducing the thermodynamic factor Γ_i

$$\frac{c_i}{RT}\nabla\mu_i = \Gamma_i \nabla c_i; \quad \Gamma_i \equiv \frac{\partial \ln f_i}{\partial \ln c_j} = \frac{c_i}{f_i}\frac{\partial f_i}{\partial c_i} \tag{4}$$

The Γ_i can be obtained by differentiating the pure component adsorption isotherm. If the adsorbed phase concentration follows a single-site Langmuir isotherm

$$c_i = c_{i,sat}\frac{b_i f_i}{1 + b_i f_i} \tag{5}$$

we get

$$\Gamma_i = \frac{1}{1 - c_i/c_{i,sat}} = \frac{1}{1 - \theta_i} \tag{6}$$

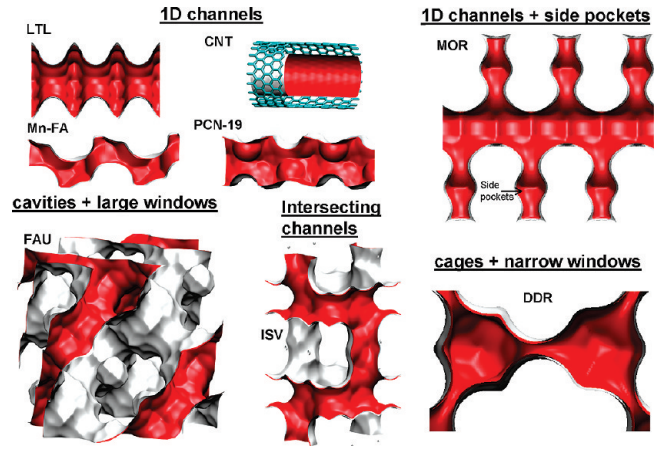

Figure 1. Examples of the variety of channel topologies and connectivities in zeolites, MOFs, COFs, and CNTs. Details of the specific structures are available in the Supporting Information accompanying this article. Here, and elsewhere in this article, we use isopotential energy surfaces as representation of porous structures; we refer the reader to Keffer et al.[191] for an explanation of how these surfaces are to be interpreted.

where we define the fractional occupancies, θ_i

$$\theta_i \equiv c_i/c_{i,sat} \tag{7}$$

Equation 6 shows that inverse thermodynamic factor, $1/\Gamma_i$, equals the fractional vacancy $(1 - \theta_i)$. In the general case, where the species adsorption exhibits inflection behavior due perhaps to second-order phase transitions, $1/\Gamma_i$ provides a good indicator of how the availability of adsorption sites changes with increased fugacity and consequently loading.

The molar density of the liquid phase is a good estimate of $c_{i,sat}$ for a variety of guest species in zeolites.[37,38] This estimation is particularly useful for light gases that have poor adsorption strength; in such cases it is difficult, if not impossible, to attain saturation conditions in adsorption isotherm measurements even when operating at high pressures.[39,40] Alternatively, GCMC simulations of the adsorption isotherms can be used for estimation of the saturation capacities, if the simulations are carried out to sufficiently high fugacities.[9] As illustration, Figure 2a−c present the GCMC simulations of the absolute loadings c_i of CH_4 for a variety of zeolites, and MOFs as a function of the bulk fluid phase fugacity, f_i. Also, shown by a continuous solid line in Figure 2a is the calculation of the fluid density, using the Peng−Robinson equation of state. For CH_4, $c_{i,sat} \approx 28-35$ kmol m^{-3}, corresponding to the density of the saturated liquid at 300 K at the pressure at which pore saturation is attained.

Inside mesopores, stepped isotherms are commonly encountered; this is a signal for capillary condensation.[41−46] For the region of loadings corresponding to the steep portion of the isotherm, the interaction of the molecules with the micropore wall serve to enhance phase stability and prevent first-order phase transitions.[42−50] The absence of capillary condensation inside micropores has been established with neutron scattering experiments;[51] these experiments also show that the molecules are present in a metastable state. The phenomenon of adsorption hysteresis is also not encountered in microporous materials, as has been demonstrated in a variety of molecular simulation studies.[42−44,50] Stepped isotherms are also possible for adsorption below critical temperatures in micropores. This is illustrated in Figure 3a for adsorption of CO_2 in IRMOF-1 at a temperature

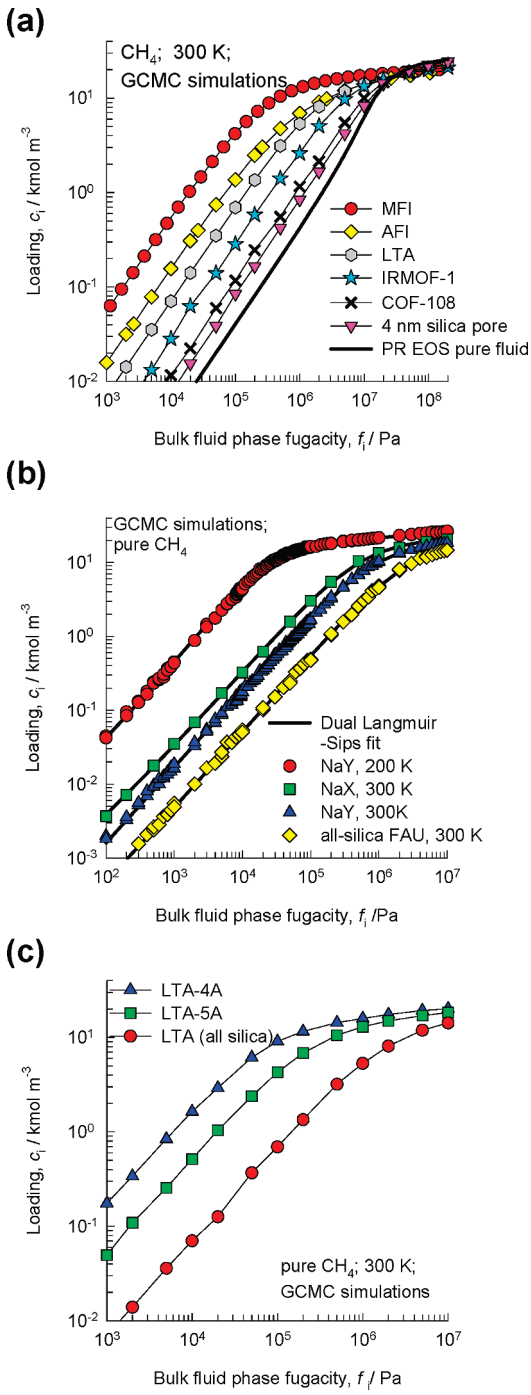

Figure 2. (a−c) GCMC simulations of adsorption isotherms for pure CH_4 in zeolites and MOFs. In (b,c) the CH_4 isotherms for FAU (all-silica) and LTA (all-silica) are compared with the corresponding structures with cations present: NaY (144 Si; 48 Al; 48 Na^+; Si/Al = 3), NaX (106 Si; 86 Al; 86 Na^+; Si/Al = 1.23), LTA-5A (96 Si; 96 Al; 32 Na^+; 32 Ca^{2+}; Si/Al = 1), and LTA-4A (96 Si; 96 Al; 96 Na^+; Si/Al = 1). The loadings are consistently expressed in terms of the concentrations in the accessible pore volume, making proper allowance for the presence of cations. Graphs are reconstructed using the data from ref 35 and augmented with additional simulations.

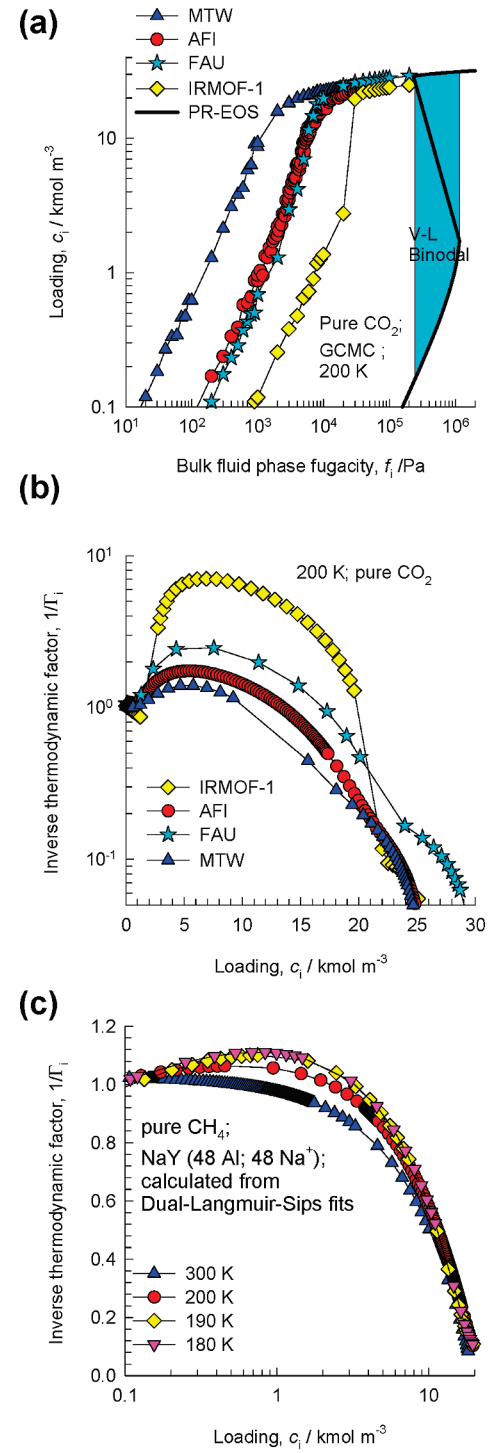

Figure 3. (a) GCMC simulations of adsorption isotherms for pure CO_2 in zeolites and MOFs at 200 K. (b) The inverse thermodynamic factor, $1/\Gamma_i$, plotted as a function of the pore loading, c_i, for adsorption of CO_2 in AFI, FAU, IRMOF-1, and MTW at 200 K. (c) The $1/\Gamma_i$ for adsorption of CH_4 in NaY at various temperatures. The $1/\Gamma_i$ is calculated by differentiation of dual-Langmuir-Sips fits of the isotherms. Graphs are reconstructed using the data from ref 52.

of 200 K, that is, below its critical temperature T_c = 304 K.[52] The steep rise in the isotherm for IRMOF-1 corresponds to the binodal vapor−liquid region, as can be evidenced by the S-shaped curve for the fluid density calculated using the Peng−Robinson equation of state. The isotherms for CO_2 at 200 K in other structures, wherein the pore size is smaller than that of IRMOF-1 do not exhibit the same degree of steepness because the interactions with the pore walls are stronger. In the metastable regions, $1/\Gamma_i$ can exceed unity even for microporous structures because of cluster formation;[52] this is illustrated by the calculations of $1/\Gamma_i$ presented in Figure 3b.

Lowering the temperature from $T > T_c$ to $T < T_c$ will have the effect of progressively increasing the steepness of the isotherm and consequently lead to $1/\Gamma_i$ values exceeding unity. This is illustrated in Figure 3c for adsorption of CH_4 in NaY. We note that for a

range of c_i, $1/\Gamma_i > 1$ when $T < T_c = 191$ K; we shall see later that a temperature decrease has a significant influence on the loading dependence of the M-S diffusivity of CH_4 in NaY.

The Fick, Onsager, and M-S diffusivities are all interrelated

$$D_i/\Gamma_i = L_i/c_i = Đ_i \tag{8}$$

By factoring out the thermodynamic influence, the $Đ_i$ can be obtained from experimental data on the Fick D_i and it is for this reason that $Đ_i$ is also referred to as the corrected diffusivity.[32] From a molecular standpoint, $Đ_i$ is a reflection of facility for collective motion of molecules and can be determined, for example, from MD simulations of displacements in each of the coordinate directions[25]

$$Đ_i = \frac{1}{2}\lim_{\Delta t\to\infty}\frac{1}{n_i}\frac{1}{\Delta t}\left\langle\left(\sum_{l=1}^{n_i}(\mathbf{r}_{l,i}(t+\Delta t)-\mathbf{r}_{l,i}(t))\right)^2\right\rangle \tag{9}$$

The M-S $Đ_i$ is amenable to simpler interpretation than the D_i because it can be related to the fundamental process of molecular jumps. The mechanism of diffusion within micropores is distinct from that within mesopores, and we begin with discussions of the former.

3. Characteristics of $Đ_i$ for Micropore Diffusion

Any molecule within a micropore cannot escape the influence of the wall interactions; and there is no "core" region for the molecule to reside in. The $Đ_i$ has a surface diffusion character.[53] Figure 1 illustrates the wide variety of channel topologies and connectivities encountered in zeolites, MOFs, COFs, and CNTs. These include one-dimensional (1D) channels (e.g., AFI, LTL, TON, CNTs, Zn(tbip),[54] MIL-47,[55] MIL-53(Cr),[56,57] PCN-19[58]), 1D zigzag channels (e.g., Co-FA,[59] Mn-FA[60]), 1D channels with side pockets (e.g., MOR, ETS-4[61]), intersecting channels (e.g., MFI, BEA, BOG, Zn(bdc)dabco,[62] Co(bdc)dabco[63]), cavities with large windows (e.g., FAU, NaX, NaY, IRMOF-1,[64] CuBTC,[65] COFs[66]), and cages separated by narrow windows (e.g., LTA, LTA-5A, LTA-4A, CHA, DDR, TSC, ERI, ITQ-29). The channel sizes of all of these structures are usually in the 0.3 to 1.5 nm range. For any guest molecule, the magnitude of $Đ_i$ and its dependence on c_i is dictated by a variety of factors including pore size, degree of confinement, topology, and connectivity.[13,35,67−71] We define the degree of confinement as the size of the molecule, characterized by the Lennard-Jones (L-J) size parameter σ, divided by the characteristic channel dimension, d_p. For the hopping of molecules across the narrow windows of structures such as LTA, CHA, and DDR, the characteristic dimension is the window size.[72] In the Supporting Information accompanying this article, the structural details for all the microporous structures that will be discussed in this article are provided, including information on the characteristic pore dimensions and the pore volume, along with simulation details and force fields used.

3.1. A Simple Model for Loading Dependence of $Đ_i$. A molecule can only jump to a site that is not occupied and the simplest model to describe the loading dependence, borrowing ideas from the theory of surface diffusion, is[53,73]

$$Đ_i = Đ_i(0)(1-\theta_i) \tag{10}$$

where $Đ_i(0)$ is the diffusivity in the limiting case of vanishingly small occupancy. We can generalize eq 10 to cater for cases

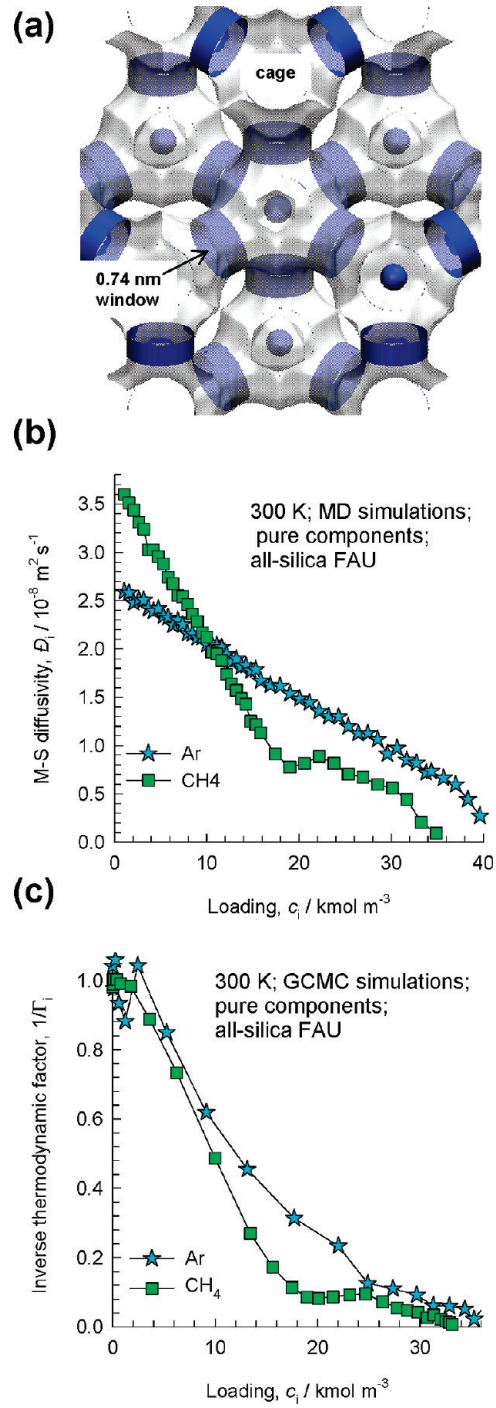

Figure 4. (a) The structure of FAU. (b) M-S diffusivity, $Đ_i$, and (c) inverse thermodynamic factor, $1/\Gamma_i$, for Ar and CH_4 in all-silica FAU as a function of the pore concentration c_i. Graphs are reconstructed using the data from refs 35, 68, and 69 augmented by additional simulations.

where the adsorbed phase does not follow simple single-site Langmuir behavior by using $1/\Gamma_i$ as a generalized measure of the fractional vacancy

$$Đ_i = Đ_i(0)\frac{1}{\Gamma_i} \tag{11}$$

This $Đ_i - c_i$ relation holds, as an approximation, for simple molecules in "open" structures such as FAU, IRMOFs, and COFs for which the degree of confinement is small, say less

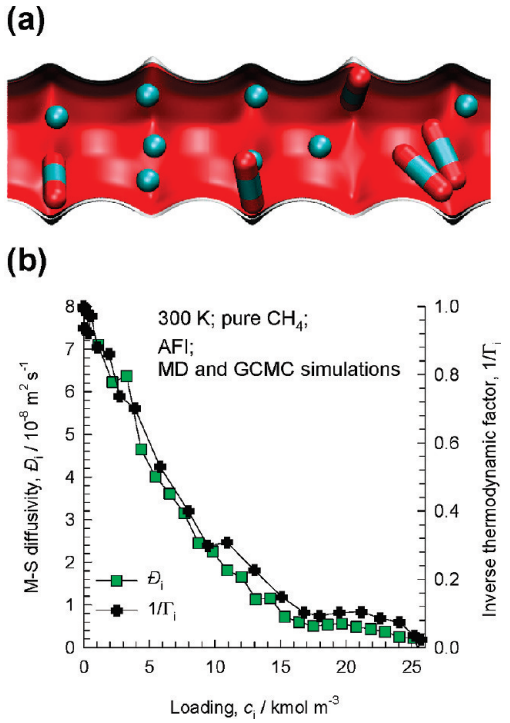

Figure 5. (a) Pore landscape of AFI. (b) M-S diffusivity, $Đ_i$, and inverse thermodynamic factor, $1/\Gamma_i$, for CH_4 in AFI as a function of the pore concentration c_i. Graph is reconstructed using the data from refs 35, 68, and 69.

than 0.4. As illustration, data for $Đ_i$ for Ar and CH_4 in FAU are shown in Figure 4b. FAU has large 0.74 nm sized windows separating cages; see Figure 4a. For Ar, $Đ_i - c_i$ is nearly linear, as would be anticipated by the linear decline in $1/\Gamma_i$ indicative of a single-site Langmuir behavior. For CH_4 the $Đ_i - c_i$ is slightly more complex and shows a mild inflection at $c_i \approx 18$ kmol m^{-3}, corresponding with the $1/\Gamma_i$ data in Figure 4c.

Equation 11 is also a reasonable approximation for lD channel structures that have pore sizes larger than about 0.7 nm, such as AFI, LTL, MIL-47, and MIL-53(Cr).[35,68,74] Figure 5 illustrates this for diffusivity of CH_4 within the 1D channels of AFI; here the $Đ_i$ and $1/\Gamma_i$ are seen to be linearly interrelated.

In cases where eq 11 holds precisely, the Fick $Đ_i$ is independent of loading. For diffusion at $T < T_c$ in concentration regions for which $1/\Gamma_i \gg 1$, the Fick $Đ_i$ may show a decreasing trend with concentration; this has been experimentally found for diffusion of alkanes in CuBTC.[65]

3.2. Isotherm Inflection Influence. In many cases the isotherm inflection is sharp, caused by preferential location of molecules within the framework. For example, branched alkanes, benzene, alkyl benzenes, and cyclohexane prefer to locate at the intersections of MFI zeolite due to extra "leg room" and other configurational considerations.[16,19,75−80] A snapshot of the location of isobutane (iC4) is shown in Figure 6a as illustration. There are only 4 intersection sites available per unit cell of MFI. This implies that to obtain loadings higher than $\Theta_i = 4$ molecules per unit cell, an extra "push" will be required to locate the molecules elsewhere within the channels; this leads to isotherm inflection. The $1/\Gamma_i$ of iC4 in MFI shows a strong inflection at a loading of $\Theta_i = 4$, when all the preferred adsorption sites are occupied; see Figure 6b. In the range $0 < \Theta_i < 4$, $1/\Gamma_i$ decreases nearly linearly with Θ_i signifying the fact that the vacancy decreases almost linearly with loading. For $4 < \Theta_i < 10$, $1/\Gamma_i$ increases with Θ_i because additional sites within the MFI channels are created to accommodate more than

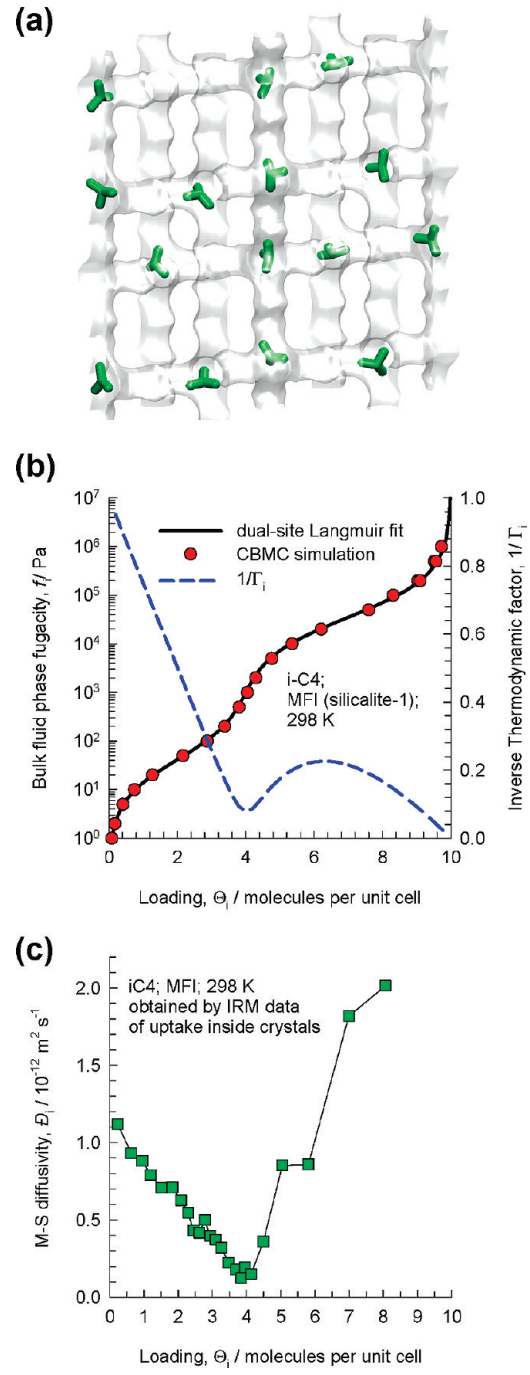

Figure 6. (a) Snapshot showing the location of iC4 in MFI at a loading of 4 molecules per unit cell. (b) Inverse thermodynamic factor, $1/\Gamma_i$, and (b) M-S diffusivity, $Đ_i$, for isobutane in MFI zeolite. Graphs are reconstructed using the data from Chmelik et al.[81]

4 molecules per unit cell, that is, the number of available sites increases within this loading range. These additional sites are located within the channels, requiring the additional "push" that caused the inflection. The $Đ_i$ data from uptake of iC4 within MFI crystals using infrared microscopy[81] shows a sharp cusplike minimum at $\Theta_i = 4$ (cf. Figure 6c), as predicted by eq 11. This cusplike $Đ_i - \Theta_i$ relation was anticipated by kinetic Monte Carlo (KMC) simulations.[82,83] The experimental data for $Đ_i$ of benzene in MFI shows similar behavior and is caused by the same reasons as illustrated for iC4.[36,84,85]

For adsorption of *n*-hexane (nC6) in MFI zeolite, the isotherm shows an inflection at $\Theta_i = 4$ because the length of a nC6 molecule is commensurate with the distance between intersec-

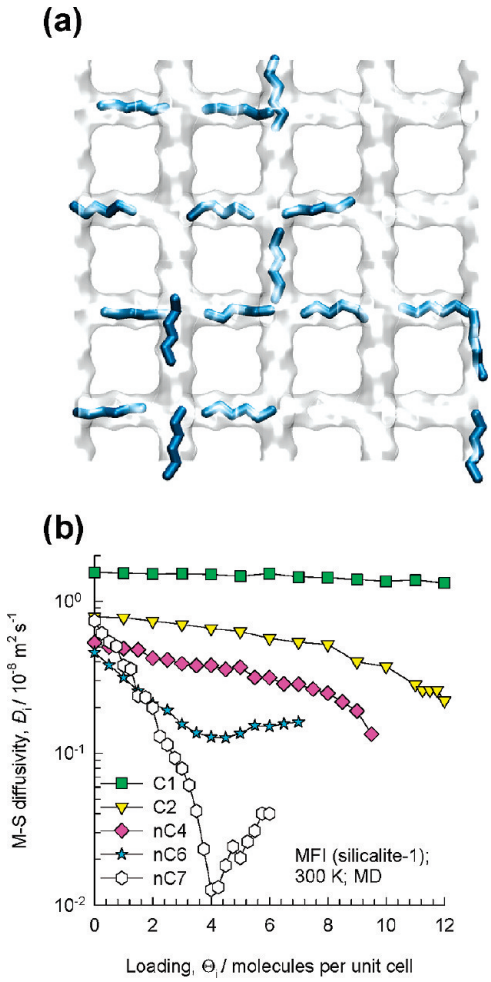

Figure 7. (a) Snapshot showing the location of nC6 in MFI at a loading of 4 molecules per unit cell. (b) MD data for $Đ_i$ of linear alkanes in MFI zeolite. Graph is reconstructed using the data from refs 88 and 192.

tions[86] (cf. snapshot in Figure 7a). The isotherm for *n*-heptane (nC7) in MFI also shows an inflection at $\Theta_i = 4$, due to the reasons discussed by Vlugt et al.[16] and Floquet et al.[87] The $Đ_i$ data of nC6 and nC7 in MFI show inflection behavior at $\Theta_i = 4$, as anticipated by eq 11; see Figure 7b. Quasi-elastic neutron scattering (QENS) experimental data of Jobic et al.[88] for diffusion of nC6 and nC7 in MFI confirm these predictions, albeit qualitatively.

Experimental $Đ_i$ data for n-alkanes in CuBTC crystals indicate the existence of metastable adsorbed phases and further underline the significant influence that $1/\Gamma_i$ exerts on the loading dependence.[65]

3.3. Hopping of Molecules Across Narrow Windows. For zeolite structures such as LTA, CHA, DDR, and ERI that consist of cages separated by narrow windows in the 0.35−0.45 nm range, a different scenario holds. A guest molecule is confined to cages separated by 8-ring windows that represent a high free-energy barrier for intercage hopping. The free energy barrier for intercage hopping, δE_i, may be defined as the difference between the values of free energy at the window and within the cages. Typical free energy profiles for CH_4 in LTA for loadings of 1 and 6 molecules per cage, are shown in Figure 8b.[70,71] We note that with increased loading, the free energy of molecules within a cage increases due to molecule−molecule interactions. As a result, δE_i decreases with increased loading (cf. Figure 8c). A consequence of the reduction of δE_i with

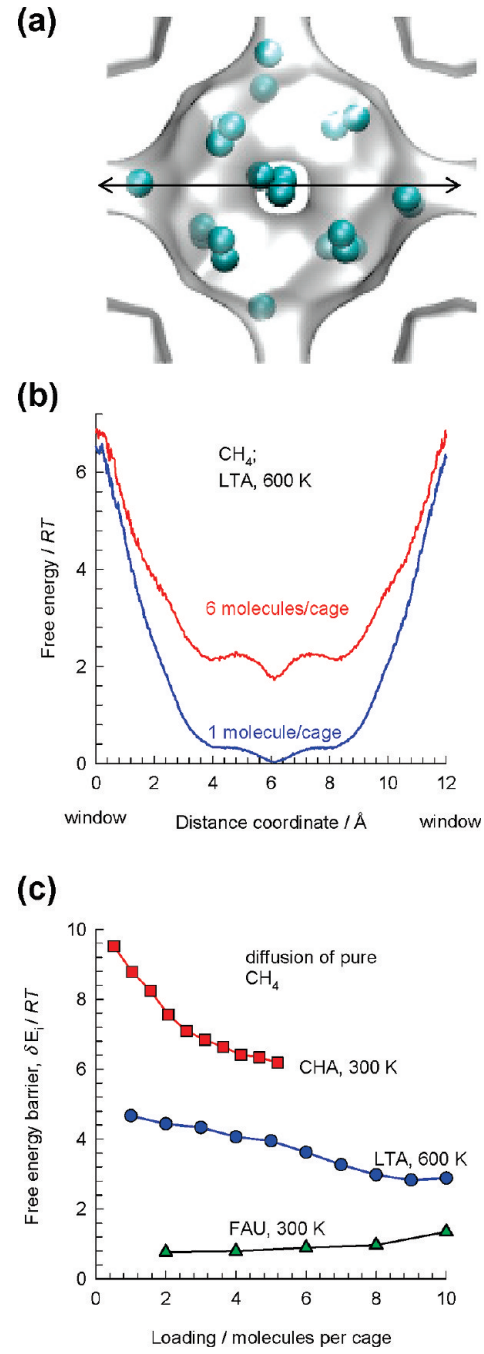

Figure 8. (a) Window-to-window distance for LTA. (b) Free energy profiles for CH_4 in LTA (all-silica) at 600 K, determined by molecular simulations for loadings of 1 and 6 molecules per cage. (c) Free energy barriers for CHA, LTA, and FAU. Graphs are based on unpublished data.

increase in occupancy, θ_i, is that $Đ_i$ increases with θ_i. The increase of $Đ_i$ with θ_i is not monotonic because the cage capacity is limited and there are fewer intracage vacant sites to occupy; also, the multiplying factor $(1 - \theta_i)$ comes into play. As the saturation loading is approached, progressively fewer vacant sites become available. The net result is that $Đ_i$ displays a maximum and decreases thereafter as $\theta_i \rightarrow 1$. For illustration of these trends, see $Đ_i$ data for Ar in LTA, CHA, DDR, and ERI in Figure 9a. More detailed discussions on the interpretation of the occupancy dependence of diffusivities in a variety of zeolite topologies on the basis of free energy profiles are available in the papers by Beerdsen et al.[70,71]

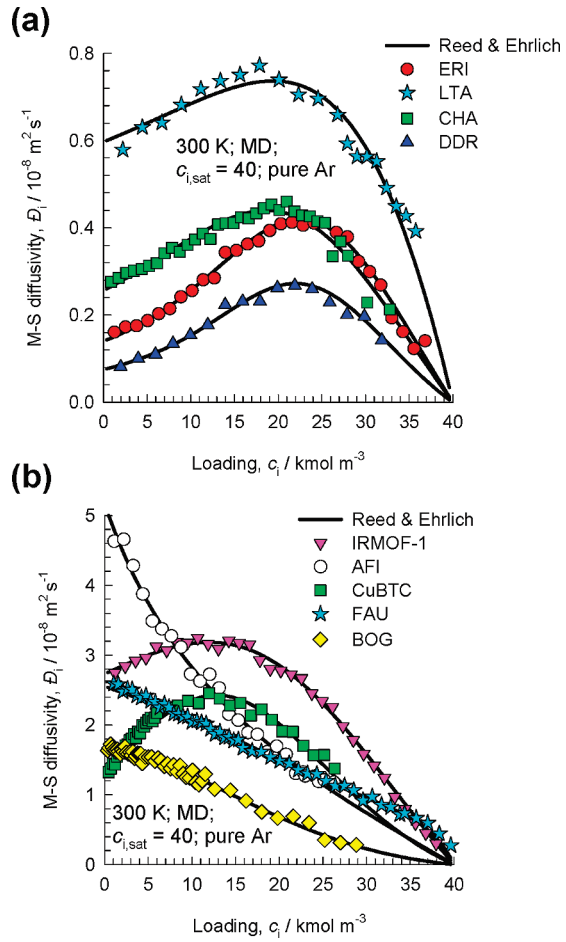

Figure 9. MD simulations of the M-S diffusivity, $Đ_i$ for Ar in (a) LTA, CHA, DDR, and ERI, and (b) IRMOF-1, AFI, BOG, and CuBTC. Also shown by continuous solid lines are the fits using the Reed and Ehrlich model with a saturation capacity $c_{i,sat} = 40$ kmol m^{-3}; in these fits $z = 5$ for 3D structures and $z = 2$ for AFI. Graphs are reconstructed using the data from refs 35, 68, and 69 augmented with additional simulations.

Equations 10 and 11 do not cater for the changes in the free-energy barrier for diffusion with increased loading and we need a more general approach to "model" the MD results in Figure 9a.

3.4. The Reed and Ehrlich Model. In the Reed and Ehrlich model[68,73,89,90] for surface diffusion of molecules obeying single-site Langmuir adsorption behavior, the intermolecular interactions within a cage are assumed to influence the hopping frequencies of molecules between cages by a factor $\phi_i = \exp(\delta E_i/RT)$ and the following expression is derived[89]

$$Đ_i = Đ_i(0)\frac{(1+\varepsilon_i)^{z-1}}{(1+\varepsilon_i/\phi_i)^z} \tag{12}$$

where z is the coordination number, representing the maximum number of nearest neighbors within a cage, and the other dimensionless parameters are

$$\varepsilon_i = \frac{(\beta_i - 1 + 2\theta_i)\phi_i}{2(1-\theta_i)}; \quad \beta_i = \sqrt{1 - 4\theta_i(1-\theta_i)(1-1/\phi_i)} \tag{13}$$

From a practical point of view, the precise choice of the value of z is not crucial, as the combination of z and ϕ_i prescribes the occupancy dependence. Since δE_i is mildly loading dependent (cf. Figure 8c), so is ϕ_i. With fitted ϕ_i, the calculations following eq 12 provide a good representation of $Đ_i - c_i$; see Figure 9a. The Reed and Ehrlich model has been used with considerable success to model experimental data on permeation of a variety of unary, binary, and ternary mixtures across and SAPO-34 and DDR membranes.[39,40,91−93] The Reed and Ehrlich model has also been used to describe the surface transport resistance of Zn(tbip) crystals.[94,95]

When the windows are large, as in the case of FAU, IRMOFs, and COFs, $\delta E_i \approx 0$ is a good approximation (cf. FAU data in Figure 8c); therefore $\phi_i \to 1$, $\beta_i = 1$, and $\varepsilon_i = \theta_i/(1-\theta_i)$, and eq 12 simplifies to eq 10.

The Reed and Ehrlich model also describes diffusion in other structures such as AFI, CuBTC, and IRMOF-1 for which the free energy barriers are difficult to define and interpret. In these cases, we simply view ϕ_i as an empirical "fit" parameter; Figure 9b illustrates the success of this approach.

The Reed and Ehrlich model in its original derivation can only handle single-site Langmuir adsorption behavior. To describe strong inflections in $Đ_i - c_i$, as witnessed for diffusion of iC4 in MFI, we may modify eq 13 by introducing $(1/\Gamma_i)$ in place of $(1-\theta_i)$

$$\varepsilon_i = \frac{(\beta_i + 1 - 2/\Gamma_i)\phi_i}{2/\Gamma_i}; \quad \beta_i = \sqrt{1 - 4(1-1/\Gamma_i)(1-1/\phi_i)/\Gamma_i} \tag{14}$$

Equations 12 and 14 reduce to eq 11 as $\phi_i \to 1$.

Equations 10, 11, 12, and 14 suggest that $Đ_i \to 0$ as $c_i \to c_{i,sat}$. In reality, the *self*-diffusivity of densely packed fluid phase is the lower limiting value for $Đ_i$ as $c_{i,sat}$ is approached. Data for the fluid phase self-diffusivities $Đ_{ii,fl}$ for a variety of pure components is shown in Figure 10a,b; the reason we use subscript "ii" to indicate the fluid phase self-diffusivity is because it reflects "self-exchange" in the fluid phase. At molar concentrations $c_i < 4$ kmol m^{-3}, the $Đ_{ii,fl}$ decreases linearly with increasing c_i; this is the low-density gas limit. For $c_i > 8$ kmol m^{-3}, we have high density fluid characteristics with a sharper decline in $Đ_{ii,fl}$ with increasing c_i. For Ar, for example, the near-vertical decline in $Đ_{ii,fl}$ occurs at 40 kmol m^{-3}, corresponding to the $c_{i,sat}$ chosen in the Reed and Ehrlich fits in Figure 9. Self-diffusivity data of CH_4 in a variety of porous materials is plotted in Figure 10c and compared with the self-diffusivity in the fluid phase, $Đ_{ii,fl}$; all data appear to decline sharply at about 30−35 kmol m^{-3}.

3.5. Factors Influencing $Đ_i(0)$. The magnitude of the diffusivity in the limit of zero loadings, $Đ_i(0)$, is influenced by a variety of factors. The most important determining factor is the degree of confinement, as evidenced in the data in Figure 11 for "spherical" guest molecules CH_4, Ar, Kr, and Ne in a variety of porous structures. At high degrees of confinement as occurs for diffusion across narrow windows of LTA, CHA, DDR, and ERI, the $Đ_i(0)$ decreases sharply by a few orders of magnitude. The $Đ_i$ simulation data for such cage-type zeolites are extremely sensitive to the choice of the L-J σ parameter; a 10% change in σ results in corresponding change in $Đ_i$ of about 2 orders of magnitude.[68] Since the parameter σ is usually tuned to match adsorption data, the predictions of diffusivities cannot be expected to be good. However, the right trends in the loading dependence are often obtained from MD simulations.[68,69,96]

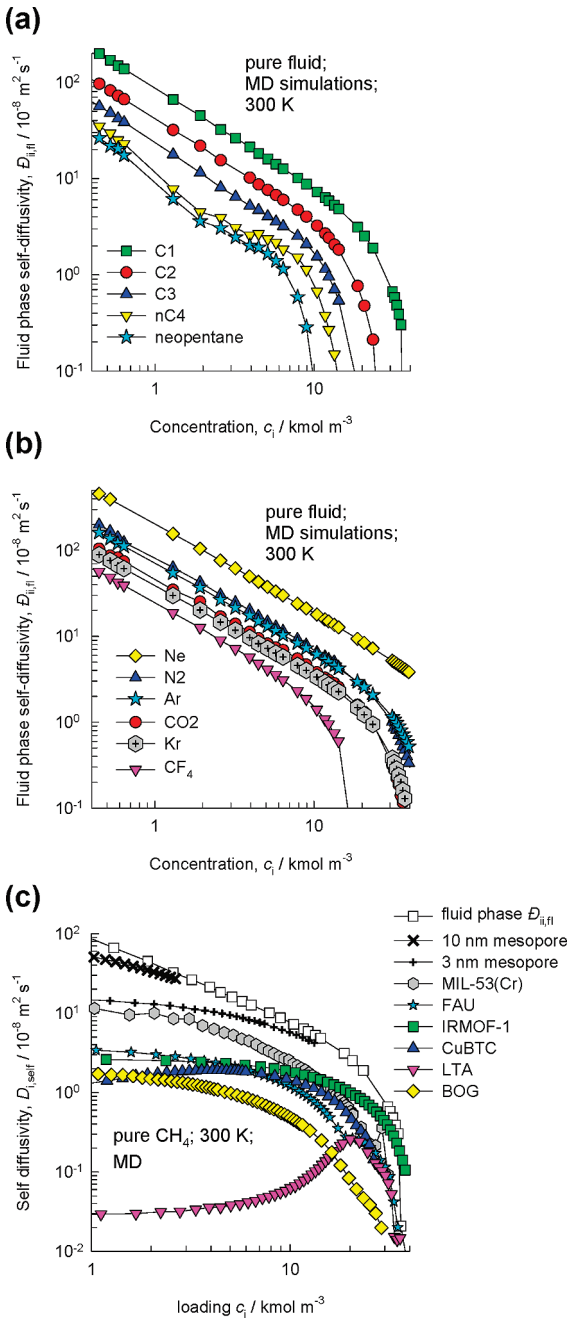

Figure 10. (a,b) Fluid phase self-diffusivity $Đ_{ii,fl}$ for pure components. (c) Self-diffusivities of CH_4 in various micro- and mesoporous materials as a function of pore concentration c_i. The graphs are reconstructed using the data from refs 35, 68, and 69 and augmented with additional simulations.

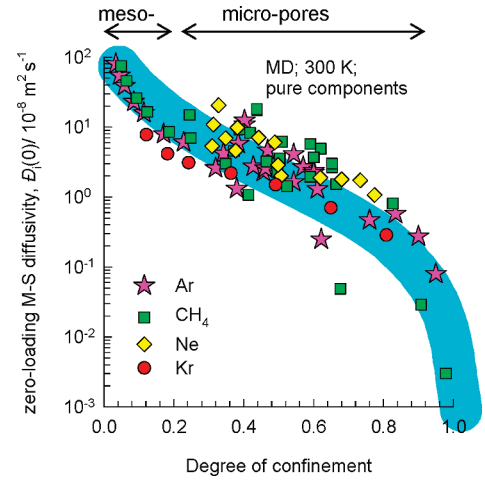

Figure 11. MD data on the M-S diffusivity at zero-loading, $Đ_i(0)$, for Ne, Ar, CH_4 and Kr, in a wide variety of zeolites, MOFs, COFs, and cylindrical silica pores, as a function of the degree of confinement, defined as σ/d_p where σ is L-J size parameter. Graph is reconstructed using the data from ref 35 augmented with additional simulations.

For "linear" molecules such as CO_2, N_2, and O_2, both the cross-sectional diameter and molecular length are influential, and it is not possible to relate diffusivity to the "kinetic" diameter as is often done in the literature.

From Figure 1, we note a periodicity in the potential energy landscape, caused by a variety of factors. For example, in LTL, TON, MTW, Co-FA, and Mn-FA there is a characteristic segment length of the 1D channels. For MFI, ISV, and BOG the periodicity is introduced by the distances between channel intersections. For LTA, DDR, CHA, and ERI the periodicity is introduced by the window-to-window distance, along with the limitation in the capacity of each cage. For diffusion of homologous series of chain molecules there could be either a match or mismatch between the characteristic periodicity of the structure and the characteristic length of the guest molecules. The net result could be a nonmonotonic variation of the diffusivity with chain length. This nonmonotonicity has been given a variety of names in the literature: resonant diffusion,[24,97,98] window effect,[99] and commensurate−incommensurate diffusion.[100−102] Some examples are given below.

If we examine the $Đ_i(0)$ data for n-alkanes in MFI zeolite as a function of the C number presented in Figure 7b, we note that the diffusivity hierarchy is C1 > C2 > nC7 > nC4 > nC6. The minimum for nC6 is because the length of the molecule is commensurate with the distance between intersections (cf. Figure 7a). We also note from Figure 7b that for loadings $\Theta_i >$ 2 there is no anomaly, and the $Đ_i$ decreases monotonically with increasing chain length when compared at the same Θ_i. Put another way, for n-alkane diffusion in MFI we could either have nonmonotonicity or not, depending on the loadings used to compare the data. This could perhaps explain why the experimental data obtained from membrane permeation[103] shows a minimum for nC6, which is in line with the MD simulations, but QENS data[24] displays a monotonous variation.

Nonmonotonicity in diffusivity can be introduced due to commensurate−incommensurate adsorption. To illustrate this, let us consider the adsorption of n-alkanes in cobalt formate (Co-FA) framework.[104] The structure has 1D zigzag channels; see the pore landscape in Figure 12a. The hierarchy of adsorption strengths for C1, C2, and C3 is as expected; increasing chain length results in higher adsorption strength; see Henry coefficient data in Figure 12b. The length of each channel segment is commensurate with that of C3 and longer molecules such as *n*-butane (nC4) and *n*-pentane (nC5), that are incommensurate and must straddle two channel segments. The incommensurate nature of adsorption is the cause of the unusual adsorption hierarchy: C3 > nC4 > nC5. n-hexane (nC6) is commensurate in length with two channel segments, and its Henry coefficient is practically the same as that for C3. The diffusivity hierarchy is the mirror image of that for the Henry coefficient; incommensurate adsorption results in a higher diffusivity value.

An analogous nonmonotonicity of $Đ_i(0)$ occurs in cage-type zeolites such as LTA, CHA, and ERI; for such zeolites the phenomenon was dubbed the "window effect" in the original publication of Gorring.[99] As illustration, conformations of nC8

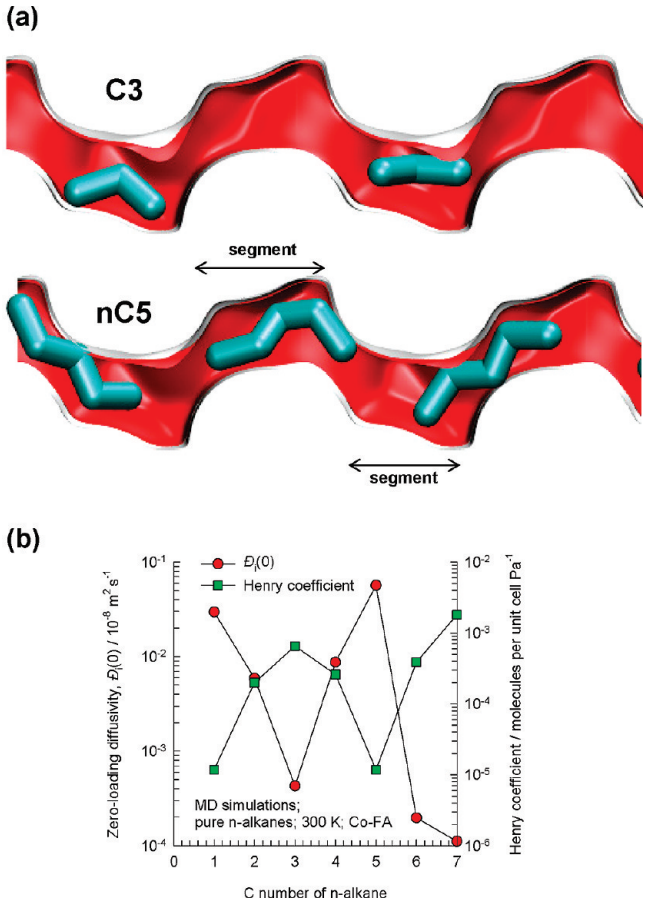

Figure 12. (a) Snapshots showing the location of C3, and nC5 alkane molecules within the zigzag 1D channels of Co-FA. (b) M-S diffusivity at zero-loading, $Đ_i(0)$, and Henry coefficient for n-alkanes in Co-FA as a function of C number. Graph is reconstructed using the data in ref 104.

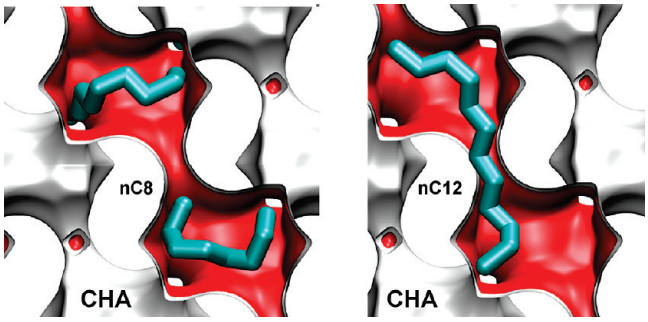

Figure 13. Snapshots showing the location of nC8 and nC12 alkane molecules within the cages of CHA.

and nC12 molecules in CHA are shown in Figure 13. nC8 is commensurate with the cage capacity; one molecule can comfortably nestle inside a cage. The longer alkane nC12 cannot fit into one cage and straddles two cages. Generally speaking, the diffusivity is higher for the incommensurate situation. Dubbeldam et al.[100−102] have investigated the window effect in a variety of cage type zeolites with the aid of rare event simulations and transition state theory and have been able to provide a fundamental understanding of the underlying phenomena.

Ruthven[105] argues that the original data of Gorring[99] are masked by thermal effects and the data can be interpreted in a different manner. While we agree with Ruthven that the Gorring data are not the proper benchmarks for validating the window effect, it does not detract from the plausibility of window effects in a variety of cage-type zeolites, as anticipated by molecular simulations.[100−102] Indeed, the QENS data of Jobic et al.[106] for diffusivity in LTA-5A show nonmonotonicity with increasing n-alkane chain length.

Besides influencing the product distribution in cracking reactions, commensurate−incommensurate phenomena can be exploited to achieve novel separations.[107,108]

3.6. Influence of Adsorption Strength. Higher adsorption strength also implies a higher "sticking" tendency, and this leads to a lower diffusivity value. As elaboration, Figure 14a,b presents data for CH_4 diffusion in FAU and LTA zeolites in which the L-J parameter for energy of interaction between CH_4 and the O atoms of the all-silica zeolites are varied in three steps, $\varepsilon/k_B = 115$ K (base case value[109]), 129 K, and 158 K (in these sensitivity studies, the L-J σ are held constant). With increasing ε/k_B the adsorption strength increases, as can be witnessed by the corresponding isotherm data in Figure 14c,d. We note that for FAU and LTA, the $Đ_i - c_i$ dependence remains "similar" as the adsorption strength increases; only the magnitude gets shifted downward.

Within MFI, the $Đ_i$ of the more strongly adsorbed CO_2 is significantly lower than that of CH_4; see Figure 15a. In MOR, the $Đ_i$ of the more strongly adsorbed CO_2 is about 2 orders of magnitude lower than that of CH_4 (cf. Figure 15b) due additionally to the preference of CO_2 to locate in the side pockets that act as cul-de-sacs[69] (cf. Figure 15c).

3.7. Influence of Cations. Consider zeolites that have Si/Al $< \infty$; in this case cations such as Na^+ and Ca^{2+} are present within the framework, preserving electroneutrality. The cations are virtually immobile and their presence increases the adsorption strength;[110,111] see for example the isotherm data for CH_4 in FAU and LTA structures in Figure 2b,c. Furthermore, the presence of cations increases the degree of confinement, because they reduce the accessible pore volume. The latter effect is accounted for implicitly in Figures 2b,c because the c_i has been defined consistently in terms of the accessible pore volume throughout this article. Both effects cause the diffusivities to be lowered; this is illustrated by the comparison of the diffusivities in FAU and NaY in Figure 16. We also note that the loading dependences in these two cases are not similar. This underlines the fact that the presence of cations does more than just increase the adsorption strength. Demontis et al.[112] report experimental data on diffusivities of H_2O in NaY and NaX that further underline the strong reduction in diffusivities with increased presence of cations.

For alkanes diffusion, the presence of Na^+ ions in MFI is found to reduce diffusivities by a factor of about 4 in the QENS data of Leroy and Jobic.[113] This reduction is more severe than for FAU because the cations not only increase the adsorption strength, but also significantly increase the degree of confinement, hindering the transport of guest molecules within the channels of MFI.

In LTA-4A, some of the Na^+ locates at the 8-membered ring window regions[72,114−116] (cf. Figure 17a) and hinder intercage hopping, thereby reducing the diffusivities to values that are too low to determine by MD. The diffusivities in this case can be determined using transition state theory (TST) calculations.[13,117] The Na^+ and Ca^{2+} cations in LTA-5A, on the other hand, do not occupy the window regions (cf. Figure 17b), and therefore intercage hopping rates are hardly affected. The reduction in CH_4 diffusivity when compared to LTA (all-silica) (cf. Figure 17c) is primarily due to the higher adsorption strength of CH_4 due to enhanced interactions with cations.

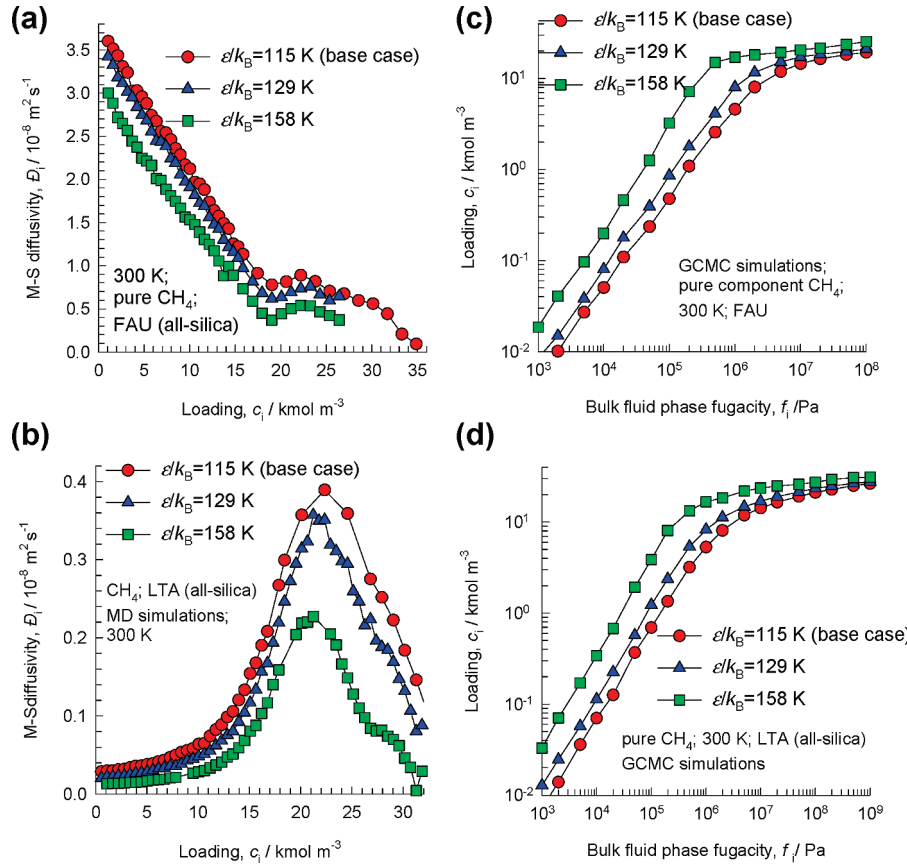

Figure 14. M-S diffusivity $Đ_i$, for pure CH_4 in (a) FAU and (b) LTA, as a function of c_i. The L-J parameter for energy of interaction between CH_4 and the O atoms of these all-silica zeolites are varied from the base case value of 115 K, $\varepsilon/k_B = 115$ K (base case), 129 K, and 158 K. In (c,d), the corresponding isotherms for FAU (all-silica) and LTA (all-silica) are presented. Graphs are constructed from unpublished data.

3.8. Influence of Temperature. Increasing temperature has two separate effects. First, a higher T causes the molecule to gain sufficient mobility to cross the barrier for activation; this causes an increase in $Đ_i$. Increasing T, relative to ε/k_B, also reduces the adsorption strength; this also has a tendency to increase $Đ_i$. But the reduction in adsorption strength is not uniform over the range of concentrations c_i. The combination of the two factors causes the loading dependence to change with T.[93] As illustration, Figure 18a presents $Đ_i - c_i$ data for CH_4 in NaY at $T = 200$ and 300 K. The data shows qualitative differences in the loading dependence; at 200 K there is a hint of a $Đ_i$ maximum at $c_i = 5$ kmol m^{-3} and a similar maximum caused by dimer formation has been reported for methanol in NaY.[118] The reason for this maximum can be traced to the fact that $1/\Gamma_i$ exhibits a slight maximum at 200 K due to incipient cluster formation; see Figure 3c.

In general, the activation energy is also loading dependent.[93] When determining activation energies for diffusion, the $Đ_i$ data should therefore be obtained at the same loading, preferably at the limit of low loadings. Since the $Đ_i$ for micropore diffusion reflects an activated process, the zero-loading diffusivities $Đ_i(0)$ show an Arrhenius temperature dependence.[31,93] For a given guest molecule, the activation energy is higher if there are cations present due to the stronger adsorption; this is exemplified by the comparison of the data for LTA (all-silica) and LTA-5A in Figure 17d.[35] Similar influences of cations are to be expected for other zeolites, and there is experimental evidence to support this contention.[31,119]

For diffusion of iC4 in MFI, Millot et al.[120,121] have calculated the activation energy by comparing the diffusivities at a constant pressure, rather than constant loading. Their experimental data shows a change in the slope of Arrhenius plot at $T = 420$ K; see Figure 18b. The loading within MFI of the branched alkane at 420 K is estimated on the basis of CBMC simulations to be $\Theta_i = 4$ molecules per unit cell. The Millot experimental data indicate different energetic behaviors below and above $\Theta_i = 4$. This change in the energetics causes differences in $Đ_i$ versus T characteristics, as has been rationalized with the aid of KMC simulations.[82]

3.9. Framework Flexibility Issues for Diffusion. Framework flexibility in zeolites usually occurs only at high temperatures and/or pressures; the change of lattice and aperture is minor because zeolite frameworks are constructed with strong covalent bonds that are rigid.[122] The assumption of a rigid framework is commonly used in MD simulations for zeolites but some theoretical pitfalls have been highlighted by Demontis.[28] Generally speaking, framework flexibility will have a bigger influence for intercage hopping across the narrow windows when the guest molecules are strongly confined, as is the case for CHA.[123]

Many MOFs possess soft "dynamic" frameworks whose cell dimensions change in a reversible manner to external stimuli. For example, IRMOF-1 exhibits negative thermal expansion.[64] Mesh adjustable molecular sieves (MAMS) allow the pore size to be precisely tailored for a given separation application by adjusting the temperature.[5] MIL-53 exhibits a "breathing effect".[57] MIL-53(Cr) has a unit cell volume of 1486 Å^3 in the as-synthesized "large pore" form (-lp). At a water loading of 2 molecules per unit cell, the unit cell volume shrinks to 1013 Å^3, the "narrow pore" (-np) form.[57] The -np structure is virtually inaccessible to guest molecules. On heating and removal of adsorbed water, the -lp form is regained. The exploitation of

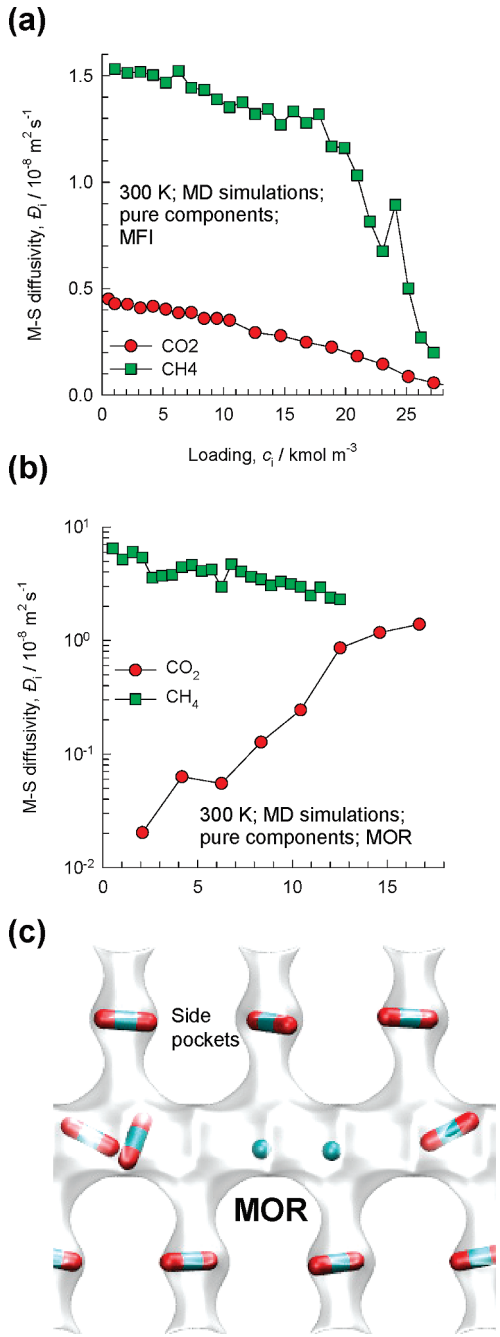

Figure 15. MD data on the M-S diffusivity for pure CH_4 and pure CO_2 in (a) MFI and (b) MOR. (c) Snapshot showing the location of CH_4 and CO_2 in MOR. The graph is reconstructed using the data from ref 69.

structural changes in MIL-53 has been suggested for purpose of controlled delivery of Ibuprofen.[124]

Lattice flexibility of IRMOF-1, which has large size cavities, has been found to increase the diffusivity by about 20−50%.[125] It may be expected that lattice flexibility will have a greater influence when the molecule is more tightly constrained within a MOF framework. For ethane diffusion at high loadings in the 0.45 nm 1D channels of Zn(tbip), MD simulations have also shown that accounting for framework flexibility leads to diffusivity values that are about 1 order of magnitude higher than for a fixed lattice.[126]

4. Characteristics of $Đ_i$ for Mesopore Diffusion

Consider diffusion of CH_4, Ar, and H_2 within a 2 nm cylindrical silica pore. The L-J interaction potential with the

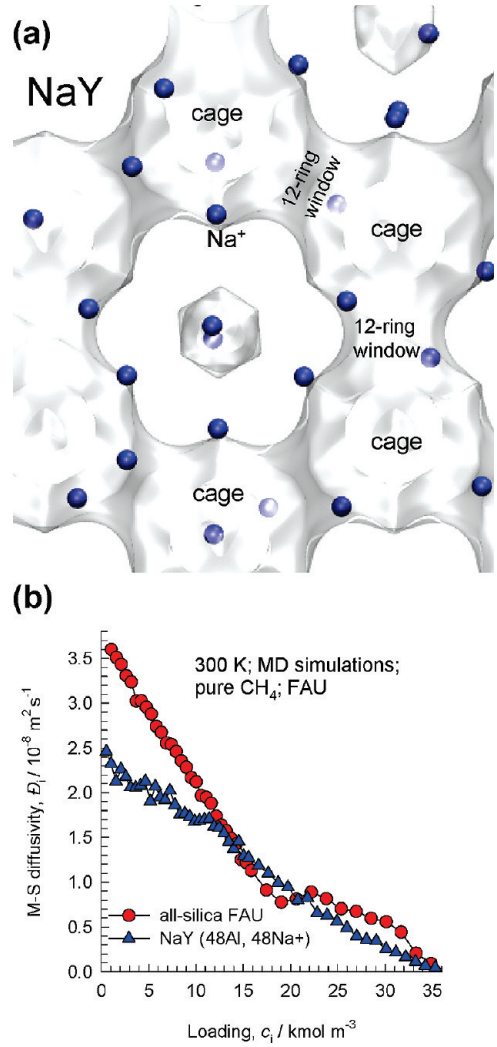

Figure 16. (a) Snapshot showing the location of Na^+ ions in NaY. (b) Data for M-S diffusivity, $Đ_i$ of CH_4 in FAU (all-silica) and NaY (144 Si; 48 Al; 48 Na^+; Si/Al = 3) at 300 K. The graph is reconstructed using the data from ref 35.

silica pore wall, normalized with respect to k_BT is shown in Figure 19. The minimum in the potential energy for interaction with the wall surface occurs at a distance $= 2^{1/6}\,\sigma$. Of the three species, CH_4 has the highest adsorption strength; the energies of interaction follow the hierarchy $CH_4 > Ar > H_2$. For distances greater than about 0.7 nm from the pore wall, the interaction potential is virtually zero for all three species. This implies that for mesoporous materials with pore sizes 2 nm < d_p < 50 nm, there is a central core region where the influence of interactions of the molecules with the pore wall is either small or negligible. Mesopore diffusion is governed by a combination of molecule−molecule and molecule−pore wall interactions.

The zero-loading diffusivity value $Đ_i(0)$ is dictated primarily by molecule−wall collisions. When the reflections are purely diffuse in nature, that is, the angle of reflection bears no relation to the angle of incidence at which the molecule strikes the pore wall, the $Đ_i(0)$ value corresponds to that obtained by the classic Knudsen formula

$$D_{i,\mathrm{Kn}} = \frac{d_p}{3}\sqrt{\frac{8RT}{\pi M_i}} \tag{15}$$

Equation 15 holds in the limiting case when the molecule does not adsorb at pore walls. Adsorption causes the molecules

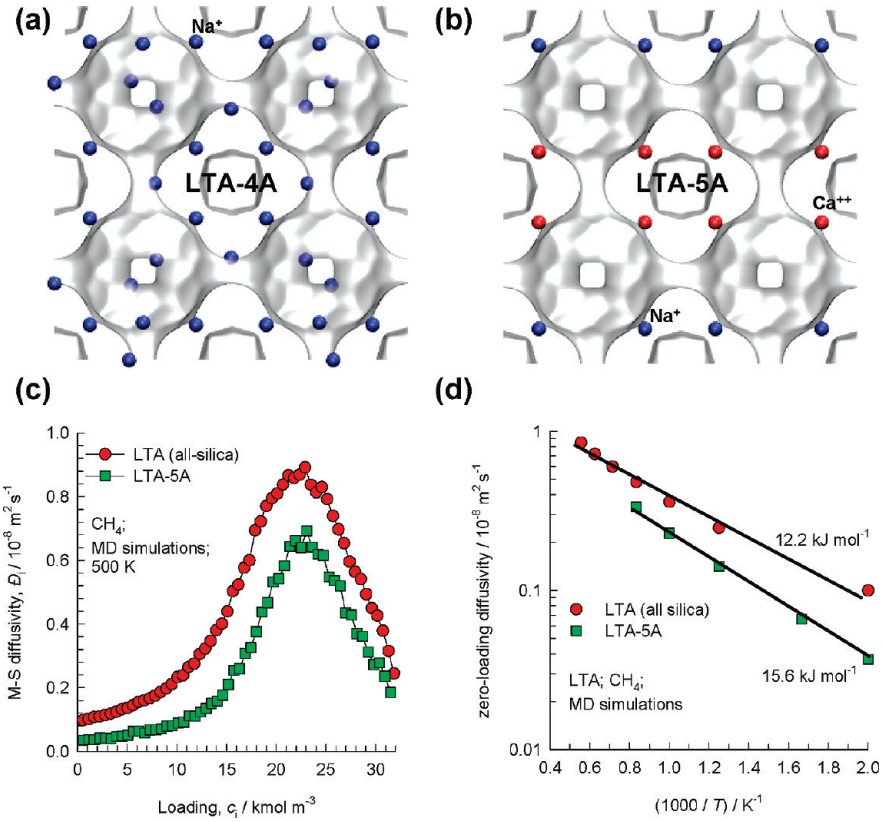

Figure 17. (a,b) Snapshots showing the location of cations in LTA-5A and LTA-4A. (c) Data for M-S diffusivity, $Đ_i$, of CH_4 in LTA (all-silica) and LTA-5A (96 Si; 96 Al; 32 Na^+; 32 Ca^{2+}; Si/Al = 1) at 500 K. (d) Arrhenius plots for LTA (all-silica) and LTA-5A. Data are from unpublished work.

to "stick" to the wall and perhaps hop to a neighboring adsorption site, rather than return to the bulk after collision.[127−129] The tendency to hop to a neighboring site on the surface is termed surface diffusion. To underline the influence of adsorption on the hopping of molecules, Figure 20 shows the trajectory that a single molecule of H_2, Ar, and CH_4 follows in a 2 nm cylindrical silica pore. The same duration of time is monitored in all three cases. The trajectory of H_2 demonstrates that a molecule that strikes the pore wall has a tendency to return to the bulk largely in keeping with the diffuse reflection scenario prescribed by the Knudsen theory. The trajectories of CH_4 are largely restricted to the region close to the pore wall because surface diffusion is dominant, and there are only occasional forays into the "core" of the pore. For Ar, the trajectory lies in between that of CH_4 and H_2; the forays into the core region are intermediate in frequency to that of CH_4 and H_2. There is a bias introduced by interactions with the wall that makes a molecule hop to a neighboring site on the surface rather than return to the bulk; this bias violates the Knudsen prescription. In the paper by Bhatia and Nicholson,[130] an oscillatory motion of adsorbed species is assumed in their model development.

In order to quantify the influence of adsorption, consider diffusion of CH_4 in a cylindrical 3 nm silica pore. MD simulations were carried out in which the L-J parameter for the energy of interaction between CH_4 and the O atoms of the silica pore are varied from the base case value of 115 K in five steps, ε/k_B = 64.6, 91.4, 115 (base case), 129, and 158 K; see Figure 21a (in these sensitivity studies, the L-J size parameter σ was held constant). With increasing ε/k_B, the adsorption strength increases, and consequently the contribution of surface diffusion increases at the expense of the Knudsen contribution; this leads to a strong decrease in the $Đ_i$. Conversely, with decreasing ε/k_B the $Đ_i$ increases and tends to approach the Knudsen diffusivity value, $D_{i,Kn} = 50 \times 10^{-8}$ m^2 s^{-1}.

In Figure 21a, the observed increase of $Đ_i$ with c_i is due to the additional contribution of viscous flow $B_0 c_i RT/\eta_i$.

Increasing temperature also reduces the adsorption strength, and results in a closer match of $Đ_i(0)$ with $D_{i,Kn}$; this is confirmed by the data for CH_4, Ar, and H_2 in 2 and 3 nm pores. In Figure 21b, the $Đ_i(0)/D_{i,Kn}$ is found to uniquely correlate with (ε/k_BT). Remarkably, the dependence of mesopore diffusivity on (ε/k_BT) was recognized already in 1958 by Lund and Berman.[131]

Experimental investigations of diffusivities of *n*-heptane, cumene, and mesitylene in mesoporous SBA-15 and SBA-16 materials have confirmed that the influence of adsorption has the effect of reducing the pore diffusivities significantly below that predicted by the Knudsen formula.[132,133] Furthermore, in these studies the activation energy for diffusion was found to have an Arrhenius character, characteristic of an activated process and in line with MD simulations.[134,135]

Ruthven et al.[136] however strikes a contradictory note and has questioned these conclusions from MD simulations by a reanalysis of the mesoporous silica membrane permeation data of Higgins et al.[137] Their reanalysis is however clouded by two factors, (1) the pore sizes are not uniform, and (2) the data for different gases are not compared at the same loading but at the same upstream membrane pressure. The loadings within the mesoporous silica membrane are not the same for the variety of gases. Consequently, the conclusions that they draw about the validity of the Knudsen theory are not definitive.

In mesoporous materials, the phenomenon of capillary condensation and adsorption hysteresis are commonly observed; these impact on diffusion.[52,65,138]

The walls of CNTs are smooth (cf. Figure 1), and the molecule-wall collisions suffer specular reflection; consequently $Đ_i(0) \gg D_{i,Kn}$.[139]

5. Describing Mixture Diffusion

To describe diffusion in n-component mixtures, we need to consider interactions between species i and species j as well. In the Onsager approach, we describe such "coupling" effects by introducing cross-coefficients

$$N_i = -\frac{1}{RT}\sum_{j=1}^{n} L_{ij}\nabla\mu_j; \quad i = 1, n \tag{16}$$

The Onsager reciprocal relations demand symmetry

$$L_{ij} = L_{ji} \tag{17}$$

The phenomenological coefficients L_{ij} are not easy to relate to the molecular-scale phenomena. A more convenient approach is to adopt the frictional formulation and generalize eq 3 by including a term to reflect "friction" between species i and species j

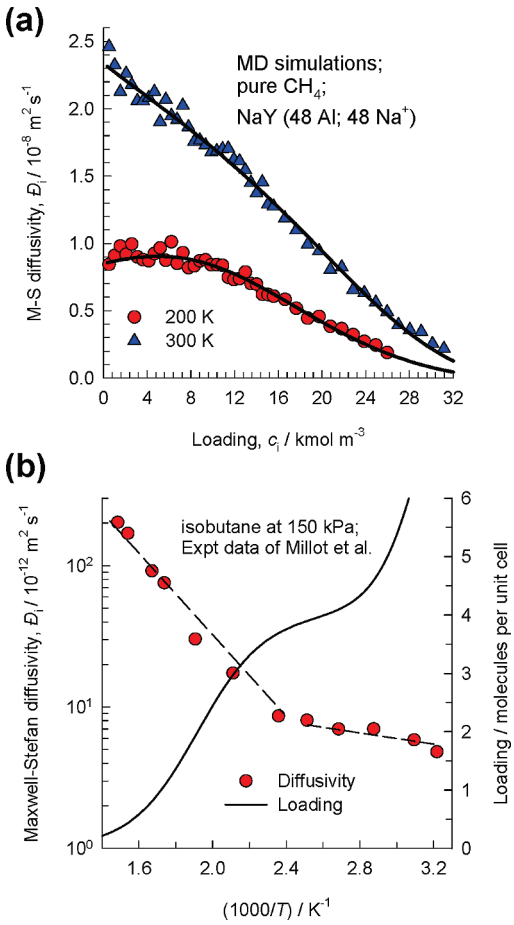

Figure 18. (a) Data for M-S diffusivity, $Đ_i$, of CH_4 in NaY (144 Si; 48 Al; 48 Na^+; Si/Al = 3) at $T = 200$ and 300 K. This graph is based on data from ref 52. (b) Arrhenius plot for the M-S diffusivity of isobutane in MFI at constant pressure of 150 kPa. Experimental data of Millot et al.[120,121] Also shown with continuous line are the sorption loadings calculated by fitting of CBMC simulated pure component isotherms.

$$-\nabla\mu_i = RT\sum_{\substack{j=1\\ j\neq i}}^{n}\frac{(u_i - u_j)}{Đ_{ij}} + RT\frac{u_i}{Đ_i}; \quad i = 1, 2, \ldots n \tag{18}$$

Equation 18 can be recast into the following form in terms of the fluxes N_i

$$-\frac{c_i}{RT}\nabla\mu_i = \sum_{\substack{j=1\\ j\neq i}}^{n}\frac{x_j N_i - x_i N_j}{Đ_{ij}} + \frac{N_i}{Đ_i}; \quad i = 1, 2, \ldots n \tag{19}$$

where x_i are the component mole fractions

$$x_i = c_i/c_t; \quad i = 1, 2, \ldots n \tag{20}$$

The origins of eqs 18 and 19 can be traced to the pioneering papers of James Clerk Maxwell[140] and Josef Stefan[141] for describing diffusion in ternary gas mixtures. Maxwell preceded Stefan in his analysis of multicomponent diffusion and the formulation should properly be termed the Maxwell−Stefan instead of Stefan−Maxwell formulation as it is sometimes referred to in the literature.[142] It is interesting to note that Stefan was aware of Maxwell's work but apparently found it difficult to follow, and remarked *Das Studium der Maxwell'schen Abhandlung ist nicht leicht* ("The study of Maxwell's treatment is not easy"). As applied to porous media transport, eq 19 was suggested first by Lightfoot[142] and subsequently used by others;[35,53,135,143,144] it does not, however, correspond with the dusty gas model,[145] that has been a subject of intense criticism in the recent literature due to some inconsistencies and handling of the viscous flow contribution.[143,144] Here, the viscous contribution is subsumed into the $Đ_i$ coefficients.

The coefficients $Đ_i$ and $Đ_{ij}$ lend themselves to easier physical interpretation than the Onsager L_{ij}. The $Đ_i$ have the same physical meaning as for unary diffusion, and characterize species i−wall interactions in the broadest sense, as discussed in the foregoing sections. The $Đ_{ij}$ are exchange coefficients representing interaction between components i with component j. At the molecular level, the $Đ_{ij}$ reflect how the facility for transport of species i correlates with that of species j. Conformity with the Onsager reciprocal relations prescribes

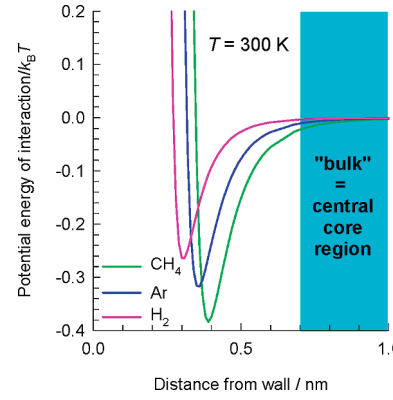

Figure 19. Normalized L-J interaction potential for CH_4 and O atoms in a silica wall surface inside a 2 nm cylindrical mesopore.

$$Đ_{ij} = Đ_{ji} \tag{21}$$

For mesopore diffusion, $Đ_{ij}$ equals the corresponding fluid phase diffusivity $Đ_{ij,fl}$, that is also accessible from independent MD simulations[35,146] or from experiment. There are reliable estimation procedures for $Đ_{ij,fl}$ using pure component properties.[147] For microporous materials, the exchange coefficient $Đ_{ij}$ defined by eq 19 cannot be directly identified with the corresponding fluid phase diffusivity $Đ_{ij,fl}$ because the species i−species j correlations are also significantly influenced by species i−wall interactions.

In earlier work,[23,68,69,148−150] the M-S formulation for micropore diffusion has been set up differently with fractional occupancies θ_i used in place of the adsorbed phase mole fractions x_i as we have done here. The important consequence of this is that the exchange coefficients $Đ_{ij}$ defined in eqs 19 have a different physical interpretation than that used in earlier work on micropore diffusion. There are persuasive advantages to using the current approach;[35] this will be further underlined in this article. The choice of either θ_i or x_i does not influence the physical interpretation of the $Đ_i$.

The M-S eqs 19 can be rewritten to evaluate the fluxes N_i explicitly

$$N_i = -\sum_{j=1}^{n} \Delta_{ij} \frac{c_j}{RT} \nabla \mu_j; \quad i = 1, 2, \ldots n \tag{22}$$

The elements Δ_{ij} of the matrix $[\Delta]$ are directly accessible from MD simulations[23−25,35,69,149,151]

$$\Delta_{ij} = \frac{1}{2} \lim_{\Delta t \to \infty} \frac{1}{n_j} \frac{1}{\Delta t} \left\langle \left(\sum_{l=1}^{n_i} (\mathbf{r}_{l,i}(t + \Delta t) - \mathbf{r}_{l,i}(t)) \right) \cdot \left(\sum_{k=1}^{n_j} (\mathbf{r}_{k,j}(t + \Delta t) - \mathbf{r}_{k,j}(t)) \right) \right\rangle \tag{23}$$

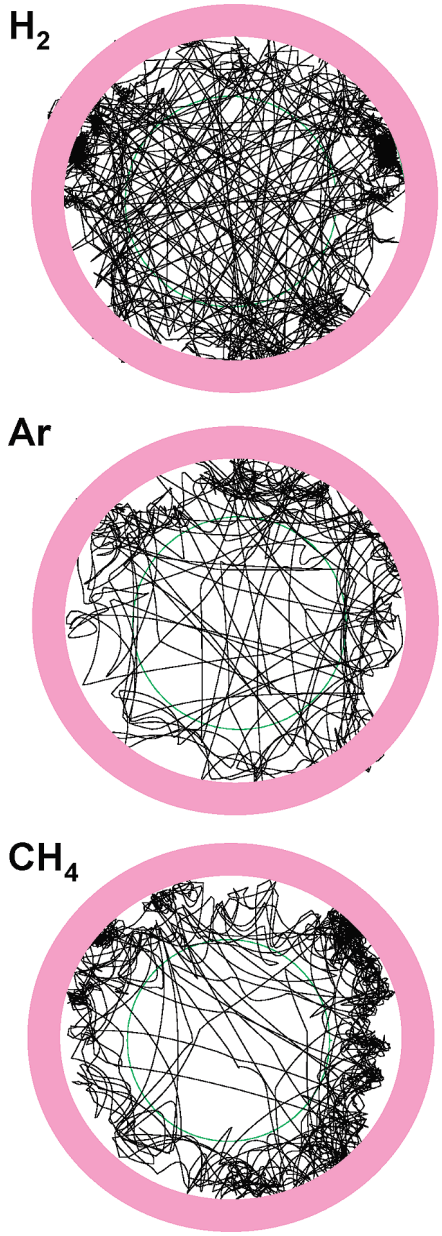

Figure 20. Trajectory of a single molecule tracked for the same duration of time during an MD simulation for diffusion of H_2, Ar, and CH_4 in a 2 nm cylindrical silica pore at 300 K. Movies tracing the path of the molecule are available as Supporting Information accompanying this article.

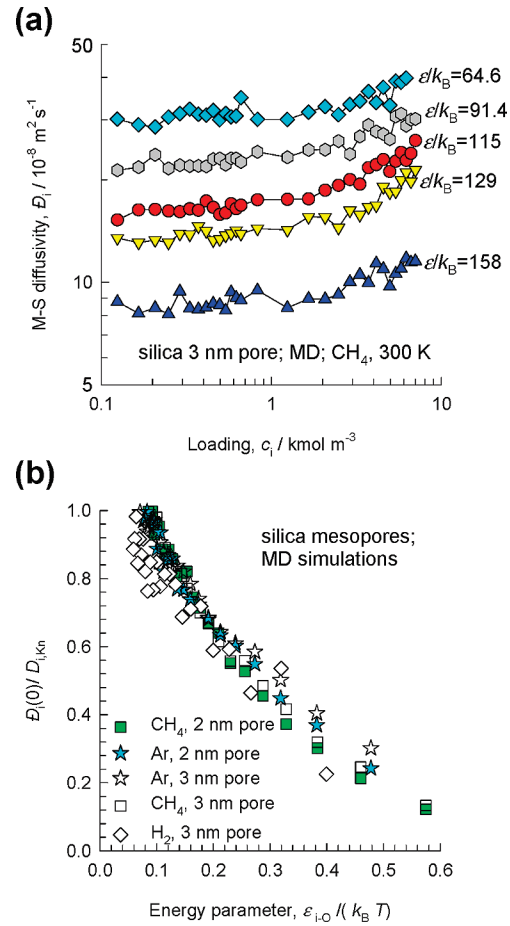

Figure 21. (a) Sensitivity study of the M-S diffusivity $Đ_i$, for diffusion of pure methane in cylindrical silica pore of 3 nm at 300 K as a function of the fluids concentration, c_i. The L-J parameter for energy of interaction between CH_4 and the O atoms of the silica pore are varied from the base case value of 115 K, $\varepsilon/k_B = 64.6$, 91.4, 115 (base case), 129, and 158 K. (b) MD data for $Đ_i(0)/D_{i,Kn}$ as a function of the energy parameter ε/k_BT for diffusion of CH_4, Ar, and H_2, at various temperatures in 2 and 3 nm cylindrical silica pores. Graphs are reconstructed using the data from refs 35 and 135.

Comparing eq 22 with eq 19 we derive the following expression for a binary mixture

$$[\Delta] = \begin{bmatrix} \frac{1}{Đ_1} + \frac{x_2}{Đ_{12}} & -\frac{x_1}{Đ_{12}} \\ -\frac{x_2}{Đ_{12}} & \frac{1}{Đ_2} + \frac{x_1}{Đ_{12}} \end{bmatrix}^{-1} \quad (24)$$

Data on the $Đ_i$ and $Đ_{ij}$ can be backed out, explicitly, from the Δ_{ij}.[35] The relationship with the Onsager coefficients is

$$\begin{bmatrix} L_{11} & L_{12} \\ L_{21} & L_{22} \end{bmatrix} = \begin{bmatrix} \Delta_{11}c_1 & \Delta_{12}c_2 \\ \Delta_{21}c_1 & \Delta_{22}c_2 \end{bmatrix} \quad (25)$$

Correlation effects influence all the L_{ij}, not just the off-diagonal elements; this is in sharp contrast with the M-S formulation in which the $Đ_i$ are free of correlation effects. Consequently, the diagonal elements L_{ii} cannot be identified with the pure component L_i, except in the special case when $L_{12} \approx 0$. By sharp contrast, in most cases the $Đ_i$ in eq 19 can be identified with the pure component value in both micro- and mesoporous materials.[35,68,69,135]

6. Self-Diffusivities and Exchange Coefficients

Let us apply eq 19 to describe equimolar diffusion ($N_1 + N_2 = 0$) in a system consisting of two species, tagged and untagged, that are identical with respect to diffusional properties

$$-\frac{c_1}{RT}\nabla\mu_1 = \frac{(x_1 + x_2)N_1}{Đ_{11}} + \frac{N_1}{Đ_1} = \left(\frac{1}{Đ_{11}} + \frac{1}{Đ_1}\right)N_1 \quad (26)$$

Equation 26 defines the self-diffusivity $D_{i,\mathrm{self}}$ within a pore

$$-\frac{c_i}{RT}\nabla\mu_i = \frac{N_i}{D_{i,\mathrm{self}}} \quad (27)$$

and we obtain

$$\frac{1}{D_{i,\mathrm{self}}} = \frac{1}{Đ_i} + \frac{1}{Đ_{ii}} \quad (28)$$

Using similar arguments, the self-diffusivities in n-component mixtures are[152]

$$\frac{1}{D_{i,\mathrm{self}}} = \frac{1}{Đ_i} + \sum_{j=1}^{n}\frac{x_j}{Đ_{ij}} = \frac{1}{Đ_i} + \frac{x_i}{Đ_{ii}} + \sum_{\substack{j=1 \\ j\neq i}}^{n}\frac{x_j}{Đ_{ij}}; \quad i = 1, 2, \ldots n \quad (29)$$

The self-diffusivity $D_{i,\mathrm{self}}$ within a pore is dictated by (a) species i−wall, (b) species i−species i, and (c) species i−species j interactions. The $D_{i,\mathrm{self}}$ can be determined from MD simulations from information on displacements of individual molecules using the formula[25]

$$D_{i,\mathrm{self}} = \frac{1}{2n_i}\lim_{\Delta t\to\infty}\frac{1}{\Delta t}\left\langle \sum_{l=1}^{n_i}(\mathbf{r}_{l,i}(t + \Delta t) - \mathbf{r}_{l,i}(t))^2 \right\rangle \quad (30)$$

At any loading $D_{i,\mathrm{self}} \leq Đ_i$; this is because individual jumps of molecules are correlated due to revisitation of sites that have been recently abandoned. The $Đ_i$, reflecting collective motion of molecules (cf. eq 9), is free from such correlation effects; it is for this reason that the $Đ_i$ are amenable to simpler interpretation and modeling than the $D_{i,\mathrm{self}}$. As examples, Figure 22 shows for $D_{i,\mathrm{self}}$ and $Đ_i$ for diffusion of CH_4 in (a) LTA, (b) MIL-53(Cr), (c) 3 nm cylindrical silica mesopore, and (d) 1.6 nm diameter CNT. The four cases are chosen to reflect four different behavioral patterns. In LTA, $D_{i,\mathrm{self}} \approx Đ_i$ except at high loadings. In cylindrical 3 nm mesopore and in the 1D channels of MIL-53(Cr), $D_{i,\mathrm{self}}$ is significantly lower than $Đ_i$. For CNT we have the extreme situation that $D_{i,\mathrm{self}}$ is 2 orders of magnitude lower than $Đ_i$. There are important consequences of these behaviors for separations, as we shall see later.

The $Đ_{ii}$ in eq 28 is the self-exchange coefficient and can be calculated from $D_{i,\mathrm{self}}$ and $Đ_i$ using eq 28. Generally speaking, the $Đ_{ii}$ are not accessible from experimental data, because it is difficult to determine both $D_{i,\mathrm{self}}$ and D_i using the same experimental technique, though QENS has been suggested as offering this possibility.[153] PFG NMR experiments yield only the $D_{i,\mathrm{self}}$. Uptake and chromatographic experiments yield $Đ_i$ after factoring out Γ_i from fitted Fick diffusivities D_i.

In the absence of pore walls, that is, in pure fluids, the molecule−molecule interactions determine the fluid phase self-diffusivity $Đ_{ii,\mathrm{fl}}$. Extensive data for $Đ_{ii}$ of a variety of molecules in mesopores ranging from 2 to 30 nm shows that $Đ_{ii} = Đ_{ii,\mathrm{fl}}$ over the entire range of loadings c_i; Figure 23a shows CH_4 data for 3 nm silica mesopore as illustration. For micropores, on the other hand molecule−molecule interactions are also strongly influenced by the interactions with the walls, and $Đ_{ii} < Đ_{ii,\mathrm{fl}}$. The reduction is by a constant factor F_i over the entire c_i range. This is demonstrated in Figure 23b with an example of diffusion of Ar within the intersecting channels of BOG; here the $Đ_{ii}$ is a fraction $F_i = 0.2$ times the value of $Đ_{ii,\mathrm{fl}}$. The extensive data[35] on F_i for a wide variety of guest−host combinations is summarized in Figure 23c; this shows a strong dependence on the degree of confinement.

The exception to the general trend in Figure 23c is the "rogue" behavior for diffusion in LTA, CHA, and DDR (the data points are encircled). These three zeolites have cages separated by narrow 0.36−0.44 nm sized windows that allow only one molecule at a time to hop from one cage to another. The intercage hopping is therefore poorly correlated,[68,69] resulting in a much higher $Đ_{ii}$, and therefore F_i, than anticipated for the narrow window size and strong confinement. Similar results hold for ERI, ITQ-29, LTA-5A, LTA-4A, and TSC. The predictions of $Đ_{ii}$ for such zeolites is however not an important issue because $D_{i,\mathrm{self}} \approx Đ_i$ is a good approximation, especially at low-to-moderate loadings; see data for LTA in Figure 22a.

Using the upper bound for the self-exchange coefficient $Đ_{ii} \leq Đ_{ii,\mathrm{fl}}$, we can derive the upper bound for the self-diffusivity is $D_{i,\mathrm{self}} \leq [(1/Đ_i) + (1/Đ_{ii,\mathrm{fl}})]^{-1} \leq Đ_{ii,\mathrm{fl}}$, as is also evidenced by the data in Figure 10c. In CNTs with smooth walls and extremely high $Đ_i$, we get $D_{i,\mathrm{self}} \approx Đ_{ii,\mathrm{fl}}$ as a good approximation.[154]

7. Degree of Correlations

The larger the value of the M-S diffusivity $Đ_i$ with respect to self-exchange $Đ_{ii}$ the stronger are the consequences of

correlation effects, and we may consider the ratio $Đ_i/Đ_{ii}$ as a measure of the degree of correlations. Figure 24 presents a summary of $Đ_i/Đ_{ii}$ data for diffusion of CH_4 in (a) cylindrical mesopores, and (b) a variety of zeolites and MOFs. The $Đ_i/Đ_{ii}$ increases with increasing c_i; this is a rational result because we may expect unsuccessful jumps, and consequent revisitation of recently abandoned sites, to increase with increasing c_i. Correlation effects are stronger in 1D and in intersecting channel structures than in larger-pore 3D "open" structures. Also, at the same c_i the $Đ_i/Đ_{ii}$ is larger in mesopores than in micropores.

For a binary mixture, correlation effects are captured by the exchange coefficient $Đ_{12}$. For a wide variety of structures investigated, the $Đ_{12}$ is found to be a factor F lower than the corresponding fluid phase $Đ_{12,fl}$[35] for which estimation procedures are well established.[147] This is illustrated in Figure 25a for diffusion of equimolar mixture of CH_4 and Ar within the intersecting channels of Zn(bdc)dabco;[62,155] here the $Đ_{12}$ is a fraction $F = 0.22$ times the fluid phase binary mixture diffusivity. The factor F shows a similar dependence on the degree of confinement as the F_i; see Figure 25b.

For a binary mixture, the exchange coefficient $Đ_{12}$ can be estimated by interpolating between the self-exchange coefficients of pure components: $Đ_{11}$ and $Đ_{22}$. On the basis of extensive MD data, the following interpolation formula, based on the Vignes[156] model for diffusion in liquid mixtures has been proposed[35]

$$Đ_{12} = (Đ_{11})^{x_1}(Đ_{22})^{x_2} \tag{31}$$

In using eq 31, the $Đ_{11}$ and $Đ_{22}$ have to be evaluated at the total mixture loading $c_t = c_1 + c_2$. Figure 25c presents an example comparison of the estimation of the eq 31 with MD simulations of $Đ_{12}$ for diffusion in an equimolar mixture of CH_4(1) and C_2H_6(2) in NaX. The good agreement is typical of a very wide variety of investigated systems.[35] Equation 31 has a transparent physical basis and is to be preferred to the interpolation formula suggested in earlier published work.[23,68,69,148−150]

In the spirit of eq 31 we may estimate the factor F for binary mixture diffusion from the pure component F_1 and F_2

$$F = (F_1)^{x_1}(F_2)^{x_2} \tag{32}$$

Use of eq 32 in conjunction with the fluid phase mixture diffusivity $Đ_{12,fl}$ provides an engineering estimate of $Đ_{12}$.

Equation 24 in combination with eq 31 and the pure component $Đ_i$ data allows the estimate of Δ_{ij}. The applicability of this approach is demonstrated in Figure 26 for diffusion of an equimolar mixture of CH_4 and CO_2 in IRMOF-1. Similar good predictions are realized for an extremely wide variety of guest−host combinations.[35] We note from the data in Figure 26 that correlations have the effect of reducing both the diagonal Δ_{ii} below the pure component $Đ_i$ value. The reduction is more severe for the more mobile CH_4. It is generally true that the more mobile the species, the more it is affected by correlations; this is because the tardier species do not vacate sites often enough.

Correlations influence the self-diffusivities in mixtures in a different way. For a binary mixture, the $D_{i,self}$ of the more mobile species is lowered due to correlations with the tardier partner. Conversely, the $D_{i,self}$ of the tardier species is increased due to

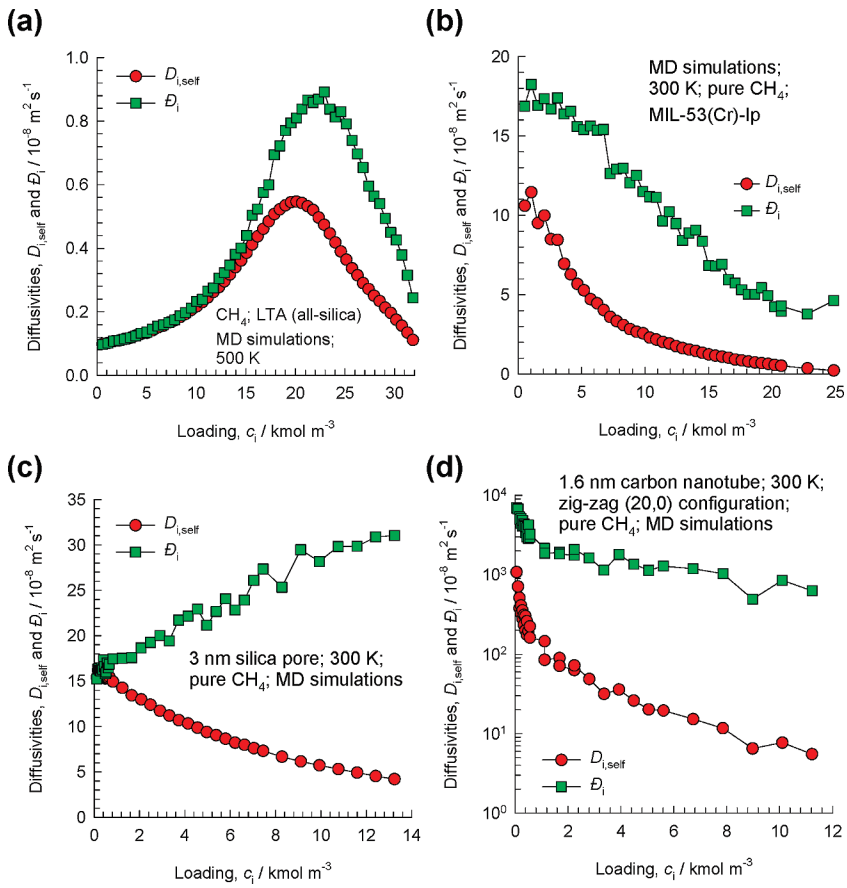

Figure 22. MD simulated data for $D_{i,self}$ and $Đ_i$ for diffusion of CH_4 in (a) LTA, (b) MIL-53(Cr) (in this case the "large pore" open structure was used), (c) 3 nm cylindrical silica mesopore, and (d) CNT (20,0) of 1.6 nm diameter. Graphs are reconstructed using the data from refs 35, 69, and 154 and augmented by additional simulations.

correlations with the more mobile partner. The net result is that the self-diffusivities of components in a mixture are closer together than the corresponding unary values. This is illustrated in Figure 27a for diffusion of C1 and C3 in NaX.

7.1. Limiting Scenarios for Mixture Diffusion. When the degree of correlations are negligibly small, that is, $Đ_i/Đ_{ij} \ll 1$, as is the case for cage-type zeolites such as LTA, CHA, ERI, and DDR, the first right member of eq 19 can be ignored and we have a set of uncoupled flux relations

$$\Delta_{ii} = Đ_i; \quad \Delta_{ij}(i \neq j) = 0; \quad N_i = -Đ_i \frac{c_i}{RT} \nabla \mu_i; \qquad \text{correlations negligible} \quad (33)$$

These uncoupled flux relations were first suggested by Habgood[157] to model uptake experiments in LTA-4A. The Habgood approximation is also a reasonable one for other structures in the limiting case of low loadings, but becomes poor for moderate loadings as illustrated in Figure 26 for CH_4-CO_2 mixture diffusion in IRMOF-1.

For transport in 1D channels correlations are particularly strong; an extreme situation occurs in CNTs for which the $Đ_i$ is a couple of orders of magnitude larger than $D_{i,\text{self}}$; see Figure 22d. This correlations-dominant case leads to the following simple expressions for binary mixtures that can be derived[69] taking $Đ_i/Đ_{ij} \gg 1$

$$\Delta_{11} = \frac{Đ_1}{1 + \frac{x_2}{x_1}\frac{Đ_1}{Đ_2}} = \Delta_{12}; \quad \Delta_{22} = \frac{Đ_2}{1 + \frac{x_1}{x_2}\frac{Đ_2}{Đ_1}} = \Delta_{21}; \qquad \text{correlations dominant} \quad (34)$$

For equimolar mixtures, $x_1 = x_2$, we get the further simplification that all elements Δ_{ij} equal one another $\Delta_{11} = \Delta_{12} = \Delta_{22} = (Đ_1Đ_2)/(Đ_1 + Đ_2)$. The calculations following this scenario are also indicated in Figure 26 for IRMOF-1, where the agreement is seen to be poor at low loadings and good at high loadings.

Equation 34 provides a good description of equimolar mixture diffusion in CNTs[69] and is a reasonable approximation for mixture diffusion in 1D channels of AFI, MIL-53(Cr), and in cylindrical mesopores.

7.2. Segregation and Hindering. There are instances where the $Đ_i$ in the mixture is different, often significantly lower, than the value of the pure component at the same pore loading.[69] This happens in cage type zeolites such as DDR, LTA, and ERI when a molecule such as CO_2 get preferentially lodged at the window region (cf. snapshot for DDR in Figure 27b), hindering the transport of partner molecules.[69,158,159]

To illustrate the influence of this hindering effect, Figure 27c presents data on self-diffusivities for CO_2 and CH_4 in DDR. For the more mobile CO_2, the values in the mixture are almost identical to that of the pure components, consistent with the negligible correlations scenario. For the tardier CH_4, the $D_{i,\text{self}}$ in the mixture are lower than the corresponding value for pure component. This lowering is not anticipated by eq 29 unless we allow for the reduction of the $Đ_i$ of CH_4 due to hindering by CO_2 lodged at the window. Such hindering effect significantly enhances the permeation selectivity for separation of CO_2 from CO_2-CH_4 and CO_2-N_2 mixtures using a DDR membrane.[158]

For $CH_4-C_2H_6$ mixture in MOR, the preferential location of CH_4 in the side pockets also causes a lowering in $Đ_i$ of CH_4 below that for the pure component.[69] When such segregation effects occur, there is a concomitant failure of the ideal adsorbed solution theory (IAST) to predict mixture phase equilibrium.[158,159] Interestingly, the consequences of segregation are more severe for mixture diffusion than for mixture adsorption.[69]

Yu et al.[160] report experimental data for transient permeation of methanol-acetone mixtures across an MFI membrane. Their

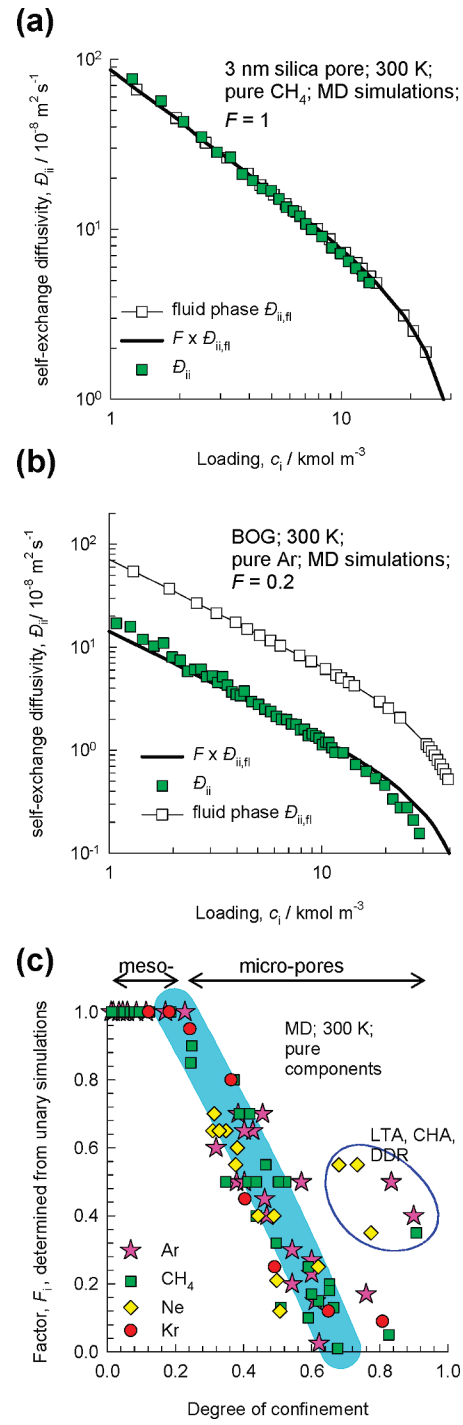

Figure 23. (a,b) The self-exchange coefficients $Đ_{ii}$ for diffusion of (a) pure CH_4 in 3 nm silca mesopore, and (b) pure Ar in BOG as a function of the pore concentration, c_i. The self-diffusivity in the fluid phase, $Đ_{ii,\text{fl}}$, obtained from independent MD simulations, are also presented in square symbols, along with continuous solid lines that represent the fraction F_i times $Đ_{ii,\text{fl}}$. (c) The factor F_i, determined from unary simulations for a wide variety of guest−host combinations, expressed as a function of the degree of confinement of guest molecules within the channels. The data for CHA, DDR, and LTA are encircled. The graphs are redrawn using the data from ref 35, augmented with additional simulations.

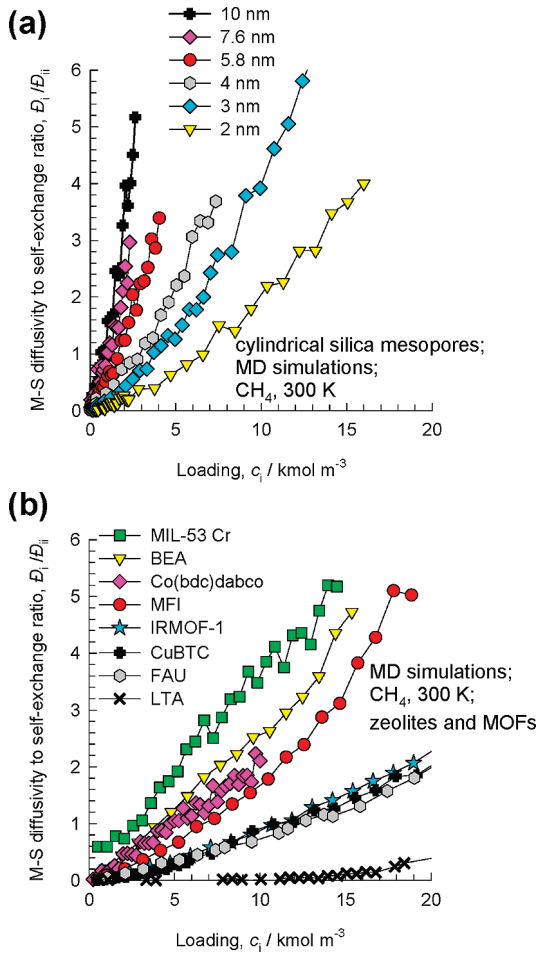

Figure 24. Ratio of the M-S diffusivity $Đ_i$ with respect to self-exchange coefficient $Đ_{ii}$ for (a) cylindrical silica mesopores with d_p = 2, 3, 4, 5.8, 7.6, and 10 nm and (b) zeolites and MOFs. Both graphs are constructed using the data from ref 35, augmented with additional simulation data.

data can only be interpreted with eq 19 by allowing both the $Đ_i$ to be lower than the corresponding pure component values. This would suggest mutual hindering of transport in the channels, a phenomenon that deserves further investigation.

8. Practical Applications

8.1. In Silico Screening of Porous Structures. Suppose we are interested in developing a membrane based process for separation of CO_2 and CH_4 and we would like to screen microporous structures that are best suited for this purpose. The permeation selectivity (= the ratio of fluxes of CO_2 and CH_4 across the membrane) is dictated both by adsorption selectivity (= ratio of loadings at the upstream face of the membrane), and the diffusion selectivity (= ratio of intracrystalline diffusivities evaluated at the total mixture loading c_t at the upstream face). For screening purposes, it is sufficient to take the ratio of self-diffusivities in the binary mixture as a measure of the diffusion selectivity.[9] Figures 28 a,b summarize the results of GCMC and MD simulations for a variety of microporous structures for typical process conditions: T = 300 K, and f_1 = f_2 = 0.5 MPa at the upstream face of the microporous membrane. The reported diffusion selectivities were determined at the loading c_t corresponding to that obtained from GCMC mixture simulations.

For all structures investigated, the CO_2 has the higher adsorption strength. We note that the best adsorption selectivities

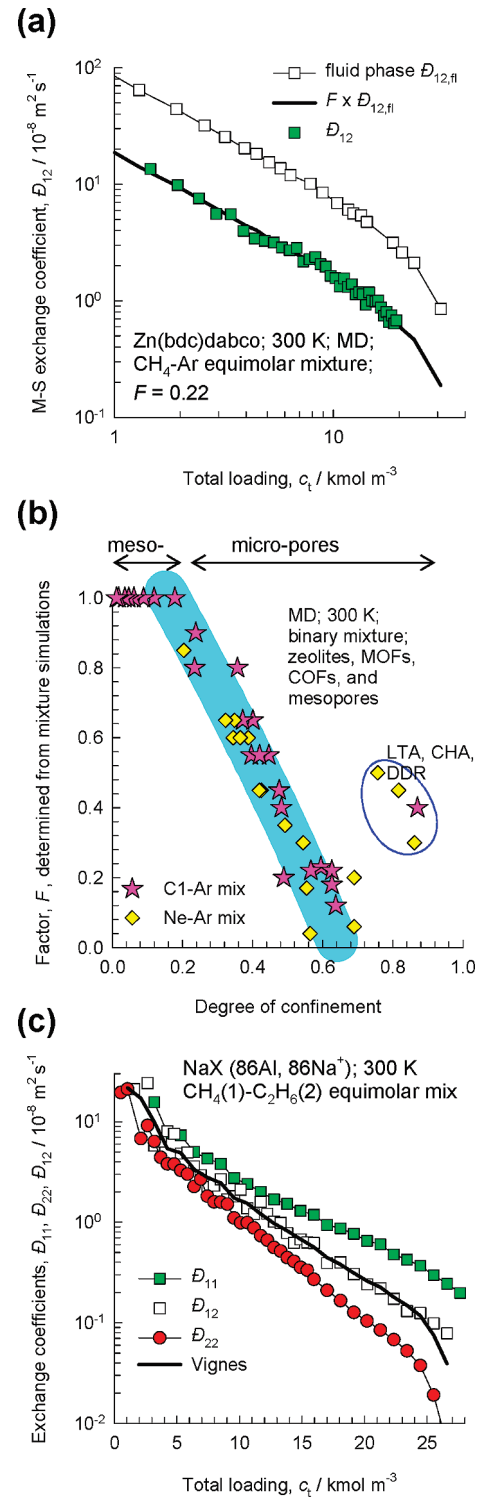

Figure 25. (a) The M-S binary exchange coefficients $Đ_{12}$, for diffusion of equimolar CH_4−Ar mixture in Zn(bdc)dabco as a function of the total concentration, c_t. The $Đ_{12,fl}$ for binary fluid phase mixture diffusion, obtained from independent MD simulations, are also presented in square symbols, along with continuous solid lines that represent the fraction F times $Đ_{12,fl}$. (b) Factor F determined from binary mixture simulations for a wide variety of zeolites, MOFs, COFs, and cylindrical silica pores. (c) Comparison of the estimation of the Vignes interpolation (eq 31), indicated by the continuous solid line, for diffusion in an equimolar mixture of CH_4(1) and C_2H_6(2) in NaX with MD simulations of $Đ_{12}$. Graphs are constructed using the data from ref 35, augmented by additional simulations.

are obtained with NaY and NaX; this is because of the enhanced adsorption strength of CO_2 due to Coulombic interactions with

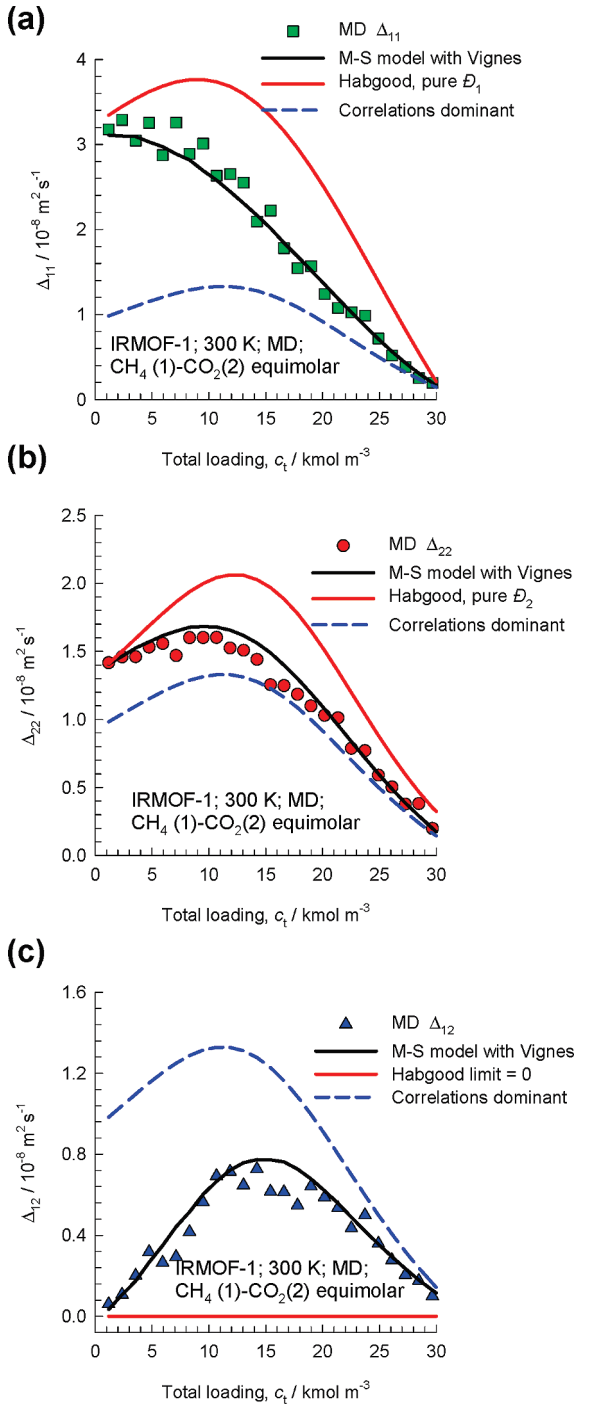

Figure 26. MD simulated values (filled symbols) of (a) Δ_{11}, (b) Δ_{22}, and (c) Δ_{12} for an equimolar mixture of CH_4 and CO_2 in IRMOF-1. The continuous lines are the predictions of eq 24, along with the Vignes interpolation formula (eq 31). Also shown are the predictions, using data determined for pure component MD simulations of $Đ_1$, and $Đ_2$, together with the Habgood approximation (eq 33) and the correlations dominant scenario (eq 34).

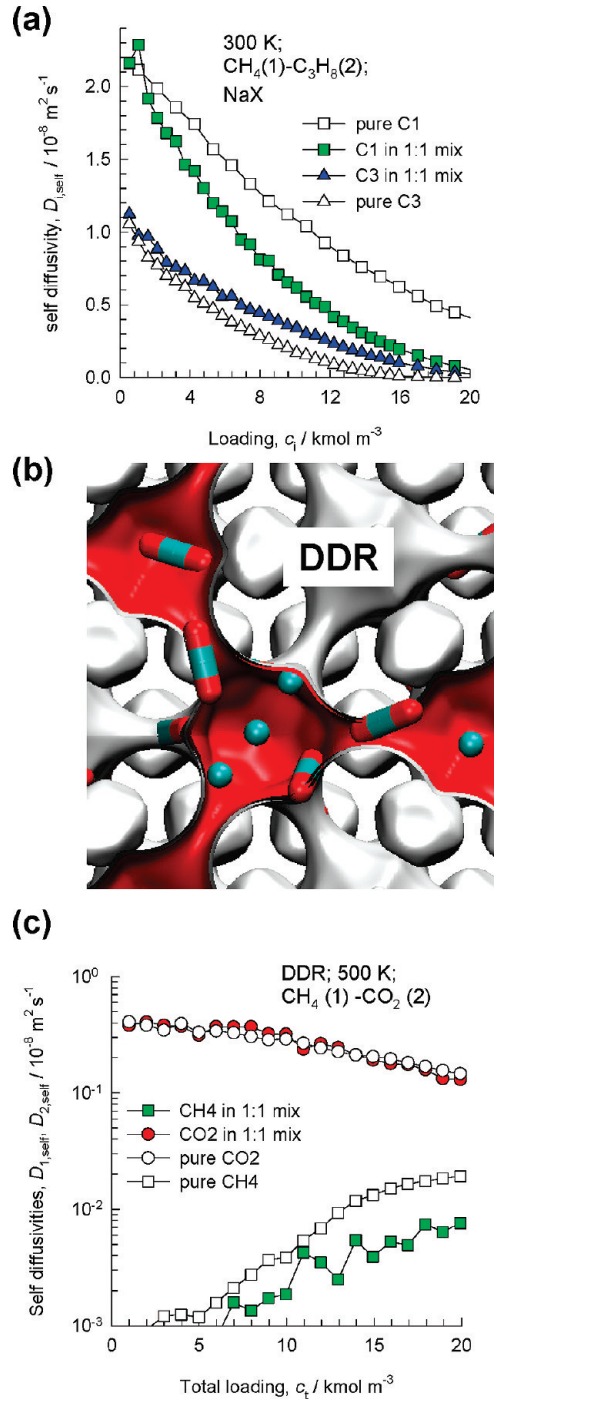

Figure 27. (a) Self-diffusivities of methane and propane in NaX. (b) Snapshots showing the location of CH_4 and CO_2 molecules in DDR. (c) Self-diffusivities of CH_4 and CO_2 in DDR. Three animations demonstrating the blocking of the window regions of DDR by CO_2, preventing diffusion of partner CH_4 molecules are available as Supporting Information accompanying this article.

the Na^+ ions. Generally speaking, however, the stronger adsorption of CO_2 leads to a poorer diffusion selectivity; indeed in structures such as FAU, NaX, NaY, and MFI, with characteristic channel sizes larger than about 0.55 nm, the diffusion selectivity is smaller than unity.

CO_2 is a more slender molecule than CH_4 and a different scenario holds for ERI, CHA, DDR, and LTA. For these structures, the diffusion selectivity is significantly higher than unity because the linear CO_2 molecule hops lengthwise across the narrow 0.35−0.45 nm sized windows. Furthermore, the preferential location of CO_2 at the window regions serves to hinder the intercage hopping of CH_4; this accounts for diffusion selectivities in excess of 20 for DDR and ERI.[158]

The product of the adsorption and diffusion selectivities yields the permeation selectivity (cf. Figure 28c), and best choices are ERI, CHA, and DDR and there is experimental evidence to support his conclusion.[9]

In silico screening strategies for microporous materials based on molecular simulation, but considering only the adsorption

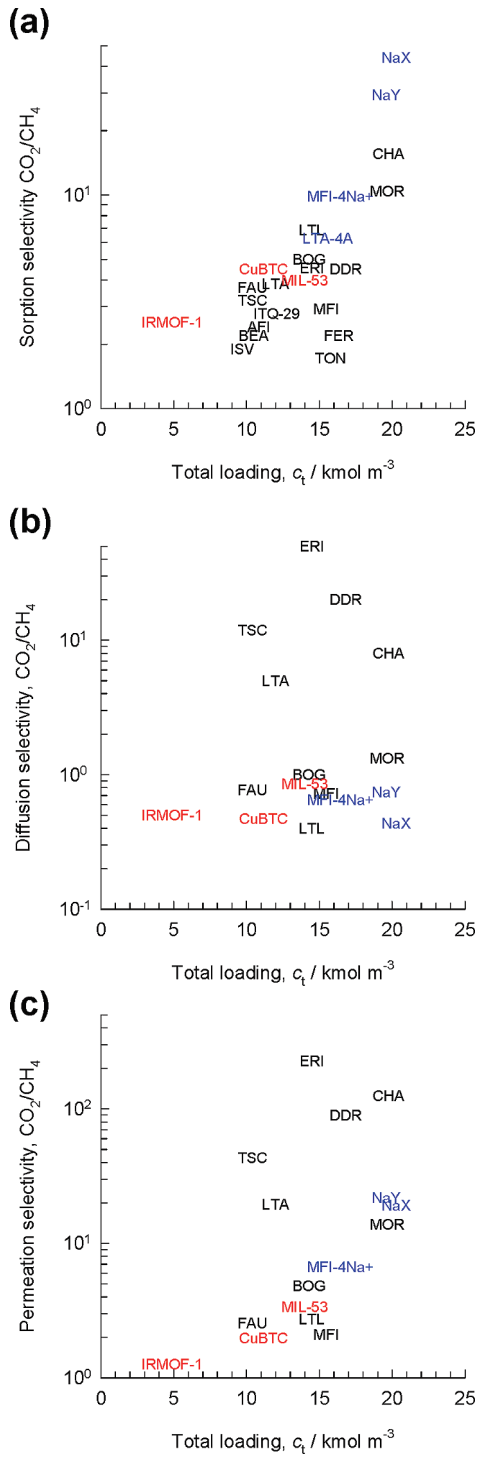

Figure 28. Selectivities for separation of CO_2 and CH_4 mixtures using a variety of microporous structures. (a) adsorption selectivity (from GCMC simulations for binary mixture taking $f_1 = f_2 = 0.5$ MPa at the upstream face), (b) diffusion selectivity ($= Đ_{1,self}/Đ_{2,self}$, evaluated at the total mixture loading at the upstream face), and (c) permeation selectivity (= product of the adsorption and diffusion selectivities). The graphs are constructed using the data from ref 9 and augmented with additional simulations.

selectivity, have been applied for separation of CO_2/CH_4, CO_2/N_2, CH_4/N_2, and hexane isomers.[77,161,162] Smit and Maesen[12,13] demonstrate how molecular simulations can be used to screen catalysts for hydrodewaxing and in innovative process development.

8.2. Modeling Permeation Across Microporous Membranes. Let us consider the permeation of CO_2 and CH_4 across an MFI membrane. Figure 29a presents the experimental data on permeation fluxes. Within the intersecting channel topology of MFI zeolite, the $Đ_i$ of CH_4 is higher than that of CO_2 (cf. Figure 15a) and therefore the permeation flux of pure CH_4 is higher than that of pure CO_2. For CO_2 (1)−CH_4 (2) mixture permeation with the equal partial pressures at the upstream face of the membrane, $p_{i,up}$, the flux of CH_4 is significantly lower than that of CO_2. There are two reasons for this. First, due to its stronger adsorption strength, the intracrystalline loadings, and driving forces, of CO_2 are higher, that is, $\nabla c_1 \gg \nabla c_2$. The second reason is that the more mobile CH_4 is slowed down due to correlated jumps within the MFI channels. Figure 29b compares the experimental CH_4 flux in the mixture with the estimations using both the two limiting scenarios, eqs 33 and 34. The Habgood model significantly overestimates the CH_4 flux because it ignores the slowing-down effect altogether. On the other hand, the correlations-dominant scenario anticipates a more severe slowing-down of CH_4 than is actually the case. For accurate predictions, better estimates of the exchange coefficients $Đ_{12}$, using eq 31, will be required. We cannot overemphasize that there is no experimental procedure to determine the $Đ_{12}$ and MD simulations are the only means to get this information.

Other MFI permeation experimental data also demonstrate the strong retarding influence exerted by tardier-but-more-strongly adsorbing species on more-mobile-but-poorly adsorbing partner molecules.[163−168]

Permeation of CO_2 and CH_4 across a SAPO-34 membrane displays markedly different characteristics. SAPO-34 is an isotype of CHA, and the $Đ_i$ value of CO_2 is about 2 orders of magnitude higher than that of CH_4 because the linear molecule jumps lengthwise across the window (cf. Figure 27b). Furthermore, the intercage hopping of molecules is practically uncorrelated and the Habgood model is applicable, as is evidenced by the comparisons of experimental fluxes with predictions following eq 33 presented in Figure 29d. The correlations-dominant scenario, eq 34, anticipates a speeding-up of the tardier CH_4, which is not realized in practice. A further noteworthy point is that the predictions of the CO_2 by either eq 33 or eq 34 are not too different, suggesting the correlations have little effect on the CO_2 flux estimations. The following result is often true: the component with significantly higher adsorption strength is less susceptible to correlations because of its preponderant concentration in the mixture; its diffusion characteristic is essentially that of the pure component. Indeed, the CO_2 flux in the mixture is practically the same as that of the pure component, when compared at the same upstream partial pressure; see Figure 29c. Conversely, the component with a significantly lower adsorption strength that is present in relatively small proportions in the mixture has its diffusion characteristics dictated by correlations with partner species with the higher loadings within the crystal. Put another way, for binary mixture permeation, estimations of the higher flux are usually more accurate than those for the smaller flux.

For modeling of permeation of CO_2/N_2, CH_4/N_2, Ar/CH_4, and $CO_2/CH_4/N_2$ mixtures across a SAPO-34 membrane, very good agreement with experiments is obtained using eq 33, for the same reasons as for CO_2/CH_4 mixture.[39,40,92] Equation 33 is also successful in describing the pervaporation of ethanol/water mixtures across an LTA-4A membrane; the rationale for the reported good agreement between model calculations and experiment is the same as for SAPO-34.[169,170]

In separation applications, correlation effects have the effect of lowering the separation selectivity. By this token, 1D channel structures such as AFI, MIL-53(Cr), and CNTs are not attractive choices for separation duties.

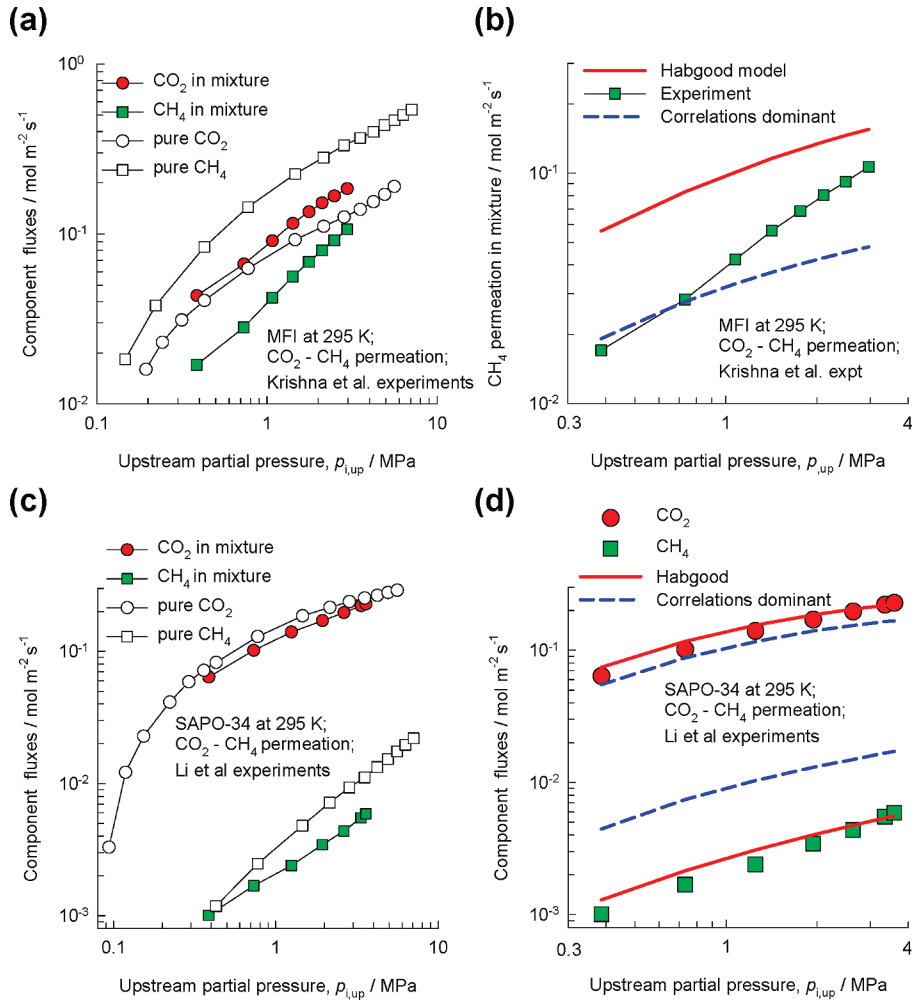

Figure 29. (a,b) Permeation fluxes for permeation of CO_2 and CH_4 across an MFI membrane as function of the component partial pressures, $p_{i,up}$, at the upstream face of the membrane.[92] (c,d) Permeation fluxes for permeation of CO_2 and CH_4 across an SAPO-34 membrane as function of the component partial pressures, $p_{i,up}$, at the upstream face of the membrane.[40] The continuous and dashed lines represent estimations of the fluxes in the mixture using the limiting scenarios, eqs 33 and 34, along with the IAST model for prediction binary adsorption equilibrium. The graphs are constructed using the data from refs 40 and 92 and augmented with additional model calculations.

8.3. Intersection Blocking and Traffic Junction Effects. In MAS PFG NMR studies, Fernandez et al.[171] found that the self-diffusivity in MFI of *n*-butane (nC4) in mixtures with isobutane (iC4) decreases to nearly zero as the loading of iC4 is increased from $\Theta_{iC4} = 0$ to 2 molecules per unit cell; see Figure 30a. The reason for this strong decline can be understood on the basis of the preferential location of iC4 at the intersections of MFI, as discussed in the context of iC4 diffusion (cf. Figure 6). For $\Theta_{iC4} = 2$, half the total number of intersections are occupied by iC4, that has a diffusivity which is about 3 orders of magnitude lower than that of nC4. Since the occupancy of the intersections is distributed randomly, each of the straight channels has an iC4 molecule ensconced somewhere along the channels; this is evident from the snapshot in Figure 30b, showing all channels have at least one iC4 molecule along its length. This is tantamount to blockage and leads to severe reduction in the molecular traffic of the intrinsically more mobile nC4. MD data on the self-diffusivity of nC4, also plotted in Figure 30a, provides confirmation of this blockage effect.[171]

Uptake experiments of Chmelik et al.[172] provide further evidence of the hindering influence iC4 has on codiffusion of nC4 in MFI. The experiments of Jiang et al.[173] demonstrate a similar strong hindering effect iC4 exerts on diffusion in MFI of mixtures with C_2H_6. PFG NMR studies of Förste et al.[174] found that the self-diffusivity of CH_4 in MFI is significantly reduced as the loading of the coadsorbed benzene increases; the explanation is again to be found in the hindering of CH_4 diffusion due to blocking of the intersections by benzene.[78,175] For analogous reasons, the branched alkanes 2-methylpentane (2MP), and 3-methylpentane (3MP), causes the reduction in the self-diffusivity of the *n*-hexane (nC6) in nC6−2MP, and nC6−3MP mixtures.[119,176] Intersection blocking by branched and cyclic hydrocarbons is a plausible explanation for the observed inhibition of the cracking of n-octane using MFI catalyst.[177]

The preferential location of branched alkanes at the intersections of MFI leads to other unusual adsorption and diffusion phenomena that can be exploited to achieve separation of hydrocarbon isomers. For illustration, consider for example a mixture of nC6 and 2,2 dimethylbutane (22DMB). Configurational-bias Monte Carlo (CBMC) simulations of the adsorbed phase loadings of the components in MFI in equilibrium with bulk fluid phase partial fugacities $f_2 = 4 f_1$ are shown in Figure 31a. Up to a total hydrocarbons fugacity f of 1 kPa, the component loadings increase in an expected manner. At $f \approx 2$ kPa, the total loading in the zeolite is ≈4 molecules per unit cell. All the intersection sites are fully occupied; see snapshot in Figure 31b. To further adsorb 22DMB, we need to provide an extra "push". Energetically, it is more efficient to obtain higher mixture loadings by "replacing" the 22DMB with nC6; this configurational entropy effect is the reason behind the

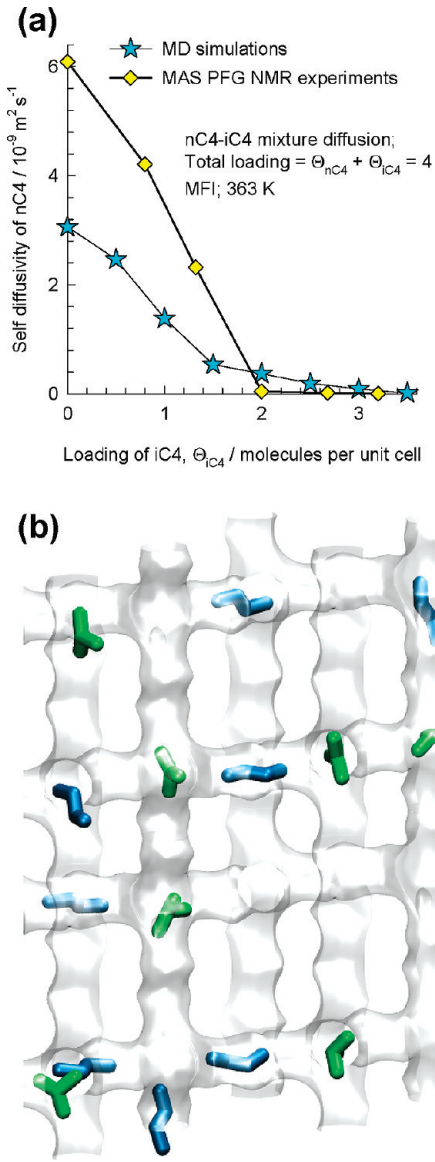

Figure 30. (a) Experimental data on self-diffusion coefficients of nC4 in nC4−iC4 mixtures in MFI as a function of the loading of iC4 in the mixture. Also shown are MD simulation data. Graph is reconstructed using the data from ref 171. (b) Snapshots showing the location of nC4 (blue) and iC4 (green) molecules in MFI.

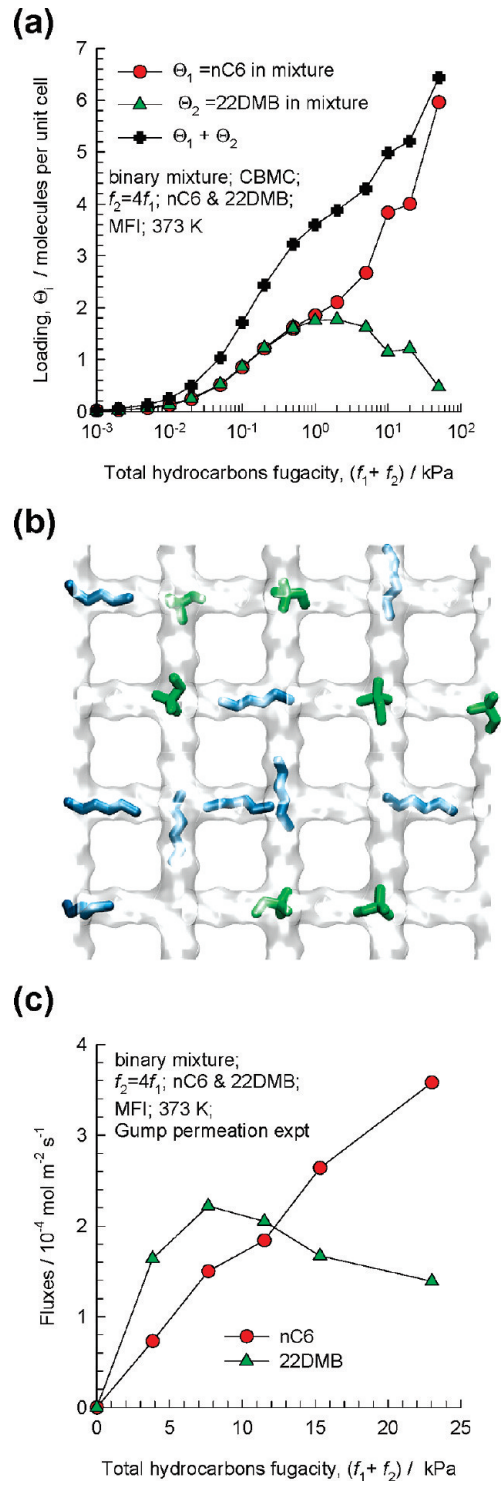

Figure 31. (a) CBMC simulations of loadings in the adsorbed phase in equilibrium with binary fluid phase containing nC6 (1)−22DMB (2) in MFI with bulk fluid fugacities $f_2 = 4 f_1$. (b) Snapshots showing the location of nC6 and 22DMB molecules in MFI. (c) Experimental data for nC6−22DMB binary mixture permeation across MFI membrane with upstream partial fugacities $f_2 = 4 f_1$. Graphs are reconstructed using the data from refs 77 and 182.

curious maxima in the 22DMB loading in the mixture at $f \approx 2$ kPa. For $f > 2$ kPa, we have the unusual phenomenon that increasing the fugacity of 22DMB in the bulk fluid phase has the effect of reducing the loading in the adsorbed phase. Experimental evidence of the curious maximum in the loading of the branched isomer is available from mixture adsorption data.[178−181] A further consequence is that for permeation of nC6−22DMB mixtures across an MFI membrane, the flux of 22DMB decreases when the upstream hydrocarbons pressures $f > 2$ kPa as observed in one set of the experiments of Gump et al.;[182] see Figure 31c. For quantitative modeling of the permeation experiments, the M-S eq 19 are required.[36,165,183]

The configuration entropy effect can be exploited to separate hydrocarbon isomers in a chromatographic column, or in a simulated moving bed adsorber.[19,168,184−186]

8.4. Diffusional Influences in Catalytic Reactions. Diffusional effects are often of vital importance in determining the effectiveness of catalysts. The classical approaches to the modeling of the catalyst effectiveness ignore the loading dependence of the diffusivities, that are characteristic of micropore diffusion, and often restricted to Langmuir−Hinshelwood (L-H) kinetic rate expressions.[187] The L-H model tacitly assumes that the saturation capacities of the component species in the mixture are all equal; consequently they do not cater for the configurational entropy effects that arise, for example, in adsorption of alkane isomers (cf. Figure 31a).[185,188,189]

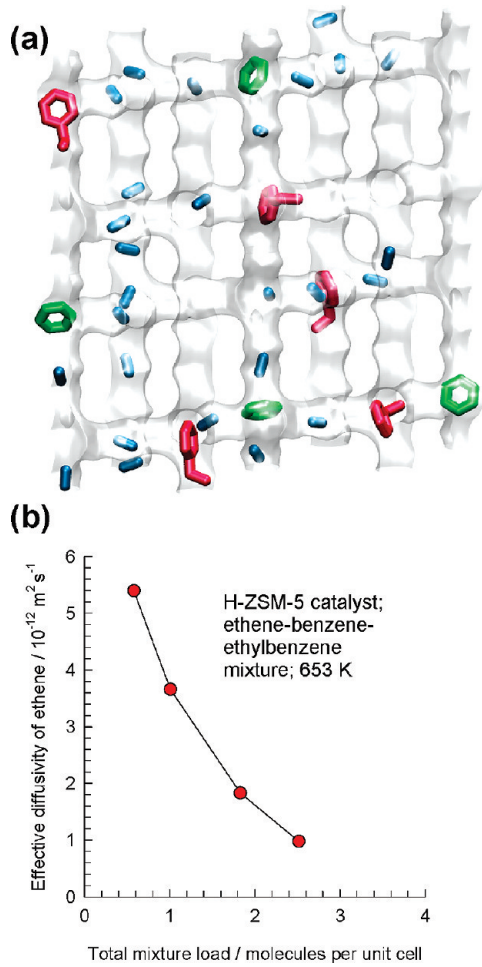

Figure 32. (a) Snapshot showing the location of reactants and products within the intersecting channel topology of MFI catalyst in the alkylation of benzene with ethene to produce ethylbenzene. (b) Effective diffusivity of ethene within MFI catalyst as a function of the mixture loading. Graph is based on data of Hansen et al.[190]

Hansen et al.[190] present a multitier theoretical study of the alkylation of benzene with ethene using MFI zeolite catalyst (in the acidic form H-ZSM-5) to produce ethylbenzene. Their paper highlights the power of modern molecular simulation tools (quantum chemical calculations and transition state theory calculations of reactivity, CBMC simulations of pure component and mixture adsorption equilibrium, MD simulations of diffusivities of pure components and mixtures) used in conjunction with the continuum models (IAST for mixture adsorption, Maxwell-Stefan eq 19, along with the Reed and Ehrlich eq 12 to describe the loading dependences) to provide a rigorous description of effectiveness of the catalyst as a function of a range of parameters (pressure, temperature, reactant feed composition). Most of the issues raised in this article apply in the description of reaction-diffusion process. Both benzene (reactant) and ethylbenzene (product) are preferentially located at the intersections of MFI (cf. snapshot in Figure 32a). This causes effective diffusivity of ethene inside the catalyst to reduce significantly as the total mixture loading approaches 2 molecules per unit cell (cf. Figure 32b), in keeping with the "traffic junction" effect explained earlier. Usual approaches to determine effectiveness factors for reactions in porous media, which assume a constant effective diffusivity, lead to substantial deviations from such a rigorous approach. The results of this study also show that empirical power law or L-H rate expressions become inappropriate when used to correlate kinetic rate data over a broad range of conditions.

9. Conclusions

The main thrust of this article has been to underline the power of molecular simulations in developing a better understanding and description of how molecules diffuse inside porous structures. The major insights gained are listed below.

(1) Equation 19 provides a convenient unified description of mixture diffusion in both micro- and mesoporous materials. The approach uses loadings c_i, expressed in terms of accessible pore volume inside the porous structures. A unified description is not possible with the more conventional approaches for micropore diffusion where the loadings are expressed in terms of moles per kg of framework.

(2) The $Đ_i$ reflects molecule−wall interactions in a broad sense. For microporous structures, the magnitude of $Đ_i$ is influenced by a variety of factors such as (a) degree of confinement, (b) adsorption strength, (c) presence of cations, and (d) commensurate−incommensurate considerations. The $Đ_i - c_i$ dependence is affected by adsorption equilibrium, isotherm inflection, and alteration in the free energy barriers for hopping of molecules. The model of Reed and Ehrlich provides a reasonable physical basis to describe $Đ_i$ versus c_i.

(3) Except in cases where we have extreme segregated adsorption within micropores, the $Đ_i$ in eq 19 can be identified with the pure component value at the loading corresponding to the total loading in the mixture, c_t.

(4) For mesoporous structures, the $Đ_i$ portrays a combination of Knudsen transport, viscous interactions, and surface diffusion characteristics. The zero-loading limit $Đ_i(0)$ corresponds to the classic Knudsen diffusivity, $D_{i,Kn}$, only when the molecules do not adsorb at the wall. With increasing adsorption $Đ_i(0)$ can be appreciably lower than $D_{i,Kn}$.

(5) The exchange coefficients $Đ_{ij}$ reflect the influence of correlations in molecular jumps. For mesopores, $Đ_{ij}$ equals the corresponding fluid phase diffusivity $Đ_{ij,fl}$, determined at the same mixture loading c_t. For micropores, the $Đ_{ij}$ is lower, by a factor F, than $Đ_{ij,fl}$. This factor F is dictated by the degree of confinement within the pores; cf. Figure 23b. Correlation effects in porous materials can be estimated using the fluid phase $Đ_{ij,fl}$ as a starting point and estimating the factor F.

(6) For binary mixtures, correlation effects cause slowing-down of the more mobile species, and speeding-up of the tardier one. Generally speaking, slowing-down effects will be significant for highly mobile, poorly adsorbing, molecules in mixtures with tardy, strongly adsorbing molecules. Speeding-up effects are generally of minor significance. Correlation effects influence, that is, reduces the selectivity of separations.

(7) For zeolite structures such as LTA, CHA, ERI, ITQ-29, TSC, and DDR consisting of cages separated by narrow windows, correlation effects are generally negligible and the uncoupled Habgood eqs 33 provide a good description of mixture diffusion.

(8) Though the Onsager and M-S approaches are formally equivalent and are derived from irreversible thermodynamics, the Onsager L_{ij} is not easily interpretable in terms of molecular scale phenomena; for this purpose, the M-S approach has overwhelming advantages.

(9) The M-S equations also provide a phenomenological description of diffusion in disordered porous materials. For such materials, there is a distribution of pore sizes with complex pore connectivities. Experimental data on the M-S diffusivities $Đ_i$, along with exchange coefficients $Đ_{ij}$, could provide clues

regarding the effective pore sizes, and also provide an indication of the pore topologies.

Acknowledgment. R.K. acknowledges the grant of a TOP subsidy from The Netherlands Foundation for Fundamental Research (NWO−CW) for intensification of reactors. Dr. J. M. van Baten is gratefully acknowledged for his assistance with the molecular simulations and preparation of the snapshots and animations. Thanks are also due to J. M. van Baten, D. Dubbeldam, and R. Q. Snurr for critically reading the manuscript.

Notation

b_i = Langmuir adsorption constant for species i, Pa^{-1}
B_O = permeability of pore, m^2
c_i = concentration of species i, mol m^{-3}
$c_{i,sat}$ = saturation capacity of species i, mol m^{-3}
c_t = total concentration in mixture, mol m^{-3}
d_p = pore diameter, m
D_i = Fick diffusivity of species i, m^2 s^{-1}
$D_{i,self}$ = self-diffusivity of species i, m^2 s^{-1}
$Đ_{ii}$ = self-exchange coefficient, m^2 s^{-1}
$Đ_{ii,fl}$ = self-diffusivity of species i in fluid phase, m^2 s^{-1}
$Đ_i$ = M-S diffusivity, m^2 s^{-1}
$Đ_i(0)$ = zero-loading M-S diffusivity, m^2 s^{-1}
$Đ_{ij}$ = M-S exchange coefficient defined by eq 19, m^2 s^{-1}
$Đ_{ij,fl}$ = M-S diffusivity in binary i-j fluid mixture, m^2 s^{-1}
$D_{i,Kn}$ = Knudsen diffusivity of species i, m^2 s^{-1}
f_i = fluid phase fugacity of species i, Pa
F = factor defined by $F \equiv Đ_{ij}/Đ_{ij,fl}$, dimensionless
F_i = factor defined by $F_i \equiv Đ_{ii}/Đ_{ii,fl}$, dimensionless
k_B = Boltzmann constant, 1.38×10^{-23} J molecule^{-1} K^{-1}
n = number of components in mixture, dimensionless
n_i = number of molecules of species i in simulation box, dimensionless
L_i = Onsager coefficients for pure component i, mol m^{-1} s^{-1}
L_{ij} = Onsager coefficients for mixture diffusion, mol m^{-1} s^{-1}
M_i = molar mass of species i, kg mol^{-1}
N_i = molar flux of species i, based on pore space, mol m^{-2} s^{-1}
p_i = partial presssure of species i, Pa
q_i = loading of i, mol kg^{-1}
$\mathbf{r}_{l,i}(t)$ = position vector for molecule l of species i at any time t, m
R = gas constant, 8.314 J mol^{-1} K^{-1}
t = time, s
T = absolute temperature, K
T_c = critical temperature, K
u_i = ensemble average velocity of species i, m s^{-1}
V_{pore} = accessible pore volume, m^3 kg^{-1}
x_i = mole fraction of species i based on loading within pore, dimensionless
z = coordination number, dimensionless

Greek Letters

β_i = Reed−Ehrlich parameter, dimensionless
Δ_{ij} = diffusivities defined by eq 22, m^2 s^{-1}
δE_i = reduction in energy barrier for diffusion, J mol^{-1}
ε = Lennard-Jones interaction energy parameter, J molecule^{-1}
ε_i = Reed−Ehrlich parameter, dimensionless
Γ_i = thermodynamic factor, dimensionless
ϕ_i = Reed−Ehrlich parameter, dimensionless
η_i = viscosity of species i, Pa s
μ_i = molar chemical potential, J mol^{-1}
θ_i = fractional occupancy of species i, dimensionless
Θ_i = loading of i, molecules per unit cell
σ = Lennard-Jones size parameter, m

Subscripts

fl = fluid phase
i = component i
t = total mixture
Kn = Knudsen
sat = saturation conditions

Vector and Matrix Notation

∇ = gradient operator
[ ] = square matrix

Supporting Information Available: (a) Document containing the pore landscapes and structural details of a variety of microporous structures (zeolites, MOFs, COFs, and CNTs) referred to in this article, along with force fields and simulation details, (b) animations showing the intercage hopping trajectories of CH_4, CO_2, and CH_4−CO_2 in DDR zeolite, and (c) animations showing the trajectories followed by H_2, Ar, and CH_4 in a 2 nm silica mesopore. This material is available free of charge via the Internet at http://pubs.acs.org.

References and Notes

(1) Davis, M. E. *Nature* **2002**, *417*, 813–821.
(2) Czaja, A. U.; Trukhan, N.; Müller, U. *Chem. Soc. Rev.* **2009**, *38*, 1284–1293.
(3) Vinu, A.; Mori, T.; Ariga, K. *Sci. Technol. Adv. Mater.* **2006**, *7*, 753–771.
(4) Pérez-Ramírez, J.; Christensen, C. H.; Egeblad, K.; Christensen, C. H.; Groen, J. C. *Chem. Soc. Rev.* **2008**, *37*, 2530–2542.
(5) Li, J. R.; Kuppler, R. J.; Zhou, H. C. *Chem. Soc. Rev.* **2009**, *38*, 1477–1504.
(6) Lee, J. Y.; Farha, O. K.; Roberts, J.; Scheidt, K. A.; Nguyen, S. T.; Hupp, J. T. *Chem. Soc. Rev.* **2009**, *38*, 1450–14594.
(7) Cohen, S. M. *Curr. Opin. Chem. Biol.* **2007**, *11*, 115–120.
(8) Férey, G.; Serre, C. *Chem. Soc. Rev.* **2009**, *38*, 1380–1399.
(9) Krishna, R.; van Baten, J. M. *Chem. Eng. J.* **2007**, *133*, 121–131.
(10) Degnan, T. F. *J. Catal.* **2003**, *216*, 32–46.
(11) Sastre, G.; Corma, A. *J. Mol. Catal. A: Chem.* **2009**, *305*, 3–7.
(12) Smit, B.; Maesen, T. L. M. *Nature* **2008**, *451*, 671–678.
(13) Smit, B.; Maesen, T. L. M. *Chem. Rev.* **2008**, *108*, 4125–4184.
(14) Maginn, E. J.; Bell, A. T.; Theodorou, D. N. *J. Phys. Chem.* **1993**, *97*, 4173–4181.
(15) Demontis, P.; Suffritti, G. B. *Chem. Rev.* **1997**, *97*, 2845–2878.
(16) Vlugt, T. J. H.; Krishna, R.; Smit, B. *J. Phys. Chem. B* **1999**, *103*, 1102–1118.
(17) Auerbach, S. M. *Int. Rev. Phys. Chem.* **2000**, *19*, 155–198.
(18) Fuchs, A. H.; Cheetham, A. K. *J. Phys. Chem. B* **2001**, *105*, 7375–7383.
(19) Krishna, R.; Smit, B.; Calero, S. *Chem. Soc. Rev.* **2002**, *31*, 185–194.
(20) Kärger, J.; Vasenkov, S.; Auerbach, S. M. Diffusion in zeolites.In *Handbook of Zeolite Science and Technology*; Auerbach, S. M., Carrado, K. A., Dutta, P. K., Eds.; Marcel Dekker: New York, 2003; Chapter 10, pp 341−422.
(21) Keffer, D. J.; Adhangale, P. *Chem. Eng. J.* **2004**, *100*, 51–69.
(22) Keffer, D. J.; Edwards, B. J.; Adhangale, P. *J. Non-Newtonian Fluid Mech.* **2004**, *120*, 41–53.
(23) Chempath, S.; Krishna, R.; Snurr, R. Q. *J. Phys. Chem. B* **2004**, *108*, 13481–13491.
(24) Jobic, H.; Theodorou, D. N. *Microporous Mesoporous Mater.* **2006**, *102*, 21–50.
(25) Dubbeldam, D.; Snurr, R. Q. *Mol. Simulation* **2007**, *33*, 15–30.
(26) Yashonath, S.; Ghorai, P. K. *J. Phys. Chem. B* **2008**, *112*, 665–686.
(27) Keskin, S.; Liu, J.; Rankin, R. B.; Johnson, J. K.; Sholl, D. S. *Ind. Eng. Chem. Res.* **2009**, *48*, 2355–2371.
(28) Demontis, P.; Suffritti, G. B. *Microporous Mesoporous Mater.* **2009**, *125*, 160–168.
(29) Frenkel, D.; Smit, B. *Understanding molecular simulations: from algorithms to applications*, 2nd ed.; Academic Press: San Diego, CA, 2002.
(30) Vlugt, T. J. H.; Van der Eerden, J. P. J. M.; Dijkstra, M.; Smit, B.; Frenkel, D. Introduction to Molecular Simulation and Statistical

Thermodynamics, Universiteit Utrecht. http://www.phys.uu.nl/~vlugt/imsst/ (accessed January 1, 2008).

(31) Kärger, J.; Ruthven, D. M. *Diffusion in zeolites and other microporous solids*; John Wiley: New York, 1992.

(32) Ruthven, D. M. *Principles of Adsorption and Adsorption Processes*; John Wiley: New York, 1984.

(33) Talu, O.; Myers, A. L. *AIChE J.* **2001**, *47*, 1160–1168.

(34) Myers, A. L.; Monson, P. A. *Langmuir* **2002**, *18*, 10261–10273.

(35) Krishna, R.; van Baten, J. M. *Chem. Eng. Sci.* **2009**, *64*, 3159–3178.

(36) Krishna, R.; Baur, R. *Sep. Purif. Technol.* **2003**, *33*, 213–254.

(37) Barrer, R. M.; Sutherland, J. W. *Proc. R. Soc. London, Ser. A* **1956**, *237*, 439–463.

(38) Golden, T. C.; Sircar, S. *J. Colloid Interface Sci.* **1994**, *162*, 182–188.

(39) Li, S.; Falconer, J. L.; Noble, R. D.; Krishna, R. *Ind. Eng. Chem. Res.* **2007**, *46*, 3904–3911.

(40) Li, S.; Falconer, J. L.; Noble, R. D.; Krishna, R. *J. Phys. Chem. C* **2007**, *111*, 5075–5082.

(41) Bhandarkar, M.; Shelekhin, A. B.; Dixon, A. G.; Ma, Y. H. *J. Membr. Sci.* **1992**, *75*, 221–231.

(42) Vishnyakov, A.; Neimark, A. V. *J. Phys. Chem. B* **2001**, *105*, 7009–7020.

(43) Neimark, A. V.; Ravikovitch, P. I.; Vishnyakov, A. *Phys. Rev. E* **2000**, *62*, R1493–R1496.

(44) Gatica, S. M.; Cole, M. W. *Phys. Rev. E* **2005**, *72*, 041602.

(45) Do, D. D.; Nicholson, D.; Do, H. D. *Mol. Simul.* **2009**, *35*, 122–137.

(46) Yasuoka, K.; Gao, G. T.; Zeng, X. C. *J. Chem. Phys.* **2000**, *112*, 4279–4285.

(47) Zarragoicoechea, G. J.; Kuz, V. A. *Phys. Rev. E* **2002**, *65*, 021110.

(48) Kholmurodov, K. T.; Yasuoka, K.; Zeng, X. C. *J. Chem. Phys.* **2001**, *114*, 9578–9584.

(49) Evans, R.; Marconi, U. M. B.; Tarazona, P. *J. Chem. Phys.* **1986**, *84*, 2376–2399.

(50) Ravikovitch, P. I.; Vishnyakov, A.; Neimark, A. V. *Phys. Rev. E* **2001**, *64*, 011602.

(51) Melnichenko, Y. B.; Wignall, G. D.; Cole, D. R.; Frielinghaus, H.; Bulavin, L. A. *J. Mol. Liq.* **2005**, *120*, 7–9.

(52) Krishna, R.; van Baten, J. M. Langmuir, submitted for publication, 2009.

(53) Krishna, R. *Chem. Eng. Sci.* **1990**, *45*, 1779–1791.

(54) Pan, L.; Parker, B.; Huang, X.; Olson, D. H.; Lee, J. Y.; Li, J. *J. Am. Chem. Soc.* **2006**, *128*, 4180–4181.

(55) Finsy, V.; Verelst, H.; Alaerts, L.; De Vos, D.; Jacobs, P. A.; Baron, G. V.; Denayer, J. F. M. *J. Am. Chem. Soc.* **2008**, *130*, 7110–7118.

(56) Coombes, D. S.; Corá, F.; Mellot-Draznieks, C.; Bell, R. G. *J. Phys. Chem. C* **2009**, *113*, 544–552.

(57) Serre, C.; Millange, F.; Thouvenot, C.; Nouguès, M.; Marsolier, G.; Louër, D.; Férey, G. *J. Am. Chem. Soc.* **2002**, *124*, 13519–13526.

(58) Ma, S.; Simmons, J. M.; Yuan, D.; Li, J. R.; Weng, W.; Liu, D. J.; Zhou, H. C. *Chem. Commun.* **2009**, 4049–4051.

(59) Li, K.; Olson, D. H.; Lee, J. Y.; Bi, W.; Wu, K.; Yuen, T.; Xu, Q.; Li, J. *Adv. Funct. Mater.* **2008**, *18*, 2205–2214.

(60) Dybtsev, D. N.; Chun, H.; Yoon, S. H.; Kim, D.; Kim, K. *J. Am. Chem. Soc.* **2004**, *126*, 32–33.

(61) Kuznicki, S. M.; Bell, V. A.; Nair, S.; Hillhouse, H. W.; Jacubinas, R. M.; Braunbarth, C. M.; Toby, B. H.; Tsapatsis, M. *Nature* **2001**, *412*, 720–724.

(62) Bárcia, P. S.; Zapata, F.; Silva, J. A. C.; Rodrigues, A. E.; Chen, B. *J. Phys. Chem. B* **2008**, *111*, 6101–6103.

(63) Wang, H.; Getzschmann, J.; Senkovska, I.; Kaskel, S. *Microporous Mesoporous Mater.* **2008**, *116*, 653–657.

(64) Dubbeldam, D.; Walton, K. S.; Ellis, D. E.; Snurr, R. Q. *Angew. Chem., Int. Ed.* **2007**, *46*, 4496–4499.

(65) Chmelik, C.; Kärger, J.; Wiebcke, M.; Caro, J.; van Baten, J. M.; Krishna, R. *Microporous Mesoporous Mater.* **2009**, *117*, 22–32.

(66) El-Kaderi, H. M.; Hunt, J. R.; Mendoza-Cortés, J. L.; Adrien P. Côté, A. P.; Robert, E.; Taylor, R. E.; O'Keeffe, M.; Yaghi, O. M. *Science* **2007**, *316*, 268–272.

(67) Skoulidas, A. I.; Sholl, D. S. *J. Phys. Chem. A* **2003**, *107*, 10132–10141.

(68) Krishna, R.; van Baten, J. M. *Microporous Mesoporous Mater.* **2008**, *109*, 91–108.

(69) Krishna, R.; van Baten, J. M. *Chem. Eng. Sci.* **2008**, *63*, 3120–3140.

(70) Beerdsen, E.; Dubbeldam, D.; Smit, B. *Phys. Rev. Lett.* **2006**, *96*, 044501.

(71) Beerdsen, E.; Dubbeldam, D.; Smit, B. *J. Phys. Chem. B* **2006**, *110*, 22754–22772.

(72) Hedin, N.; DeMartin, G. J.; Roth, W. J.; Strohmaier, K. G.; Reyes, S. C. *Microporous Mesoporous Mater.* **2008**, *109*, 327–334.

(73) Reed, D. A.; Ehrlich, G. *Surf. Sci.* **1981**, *102*, 588–609.

(74) Krishna, R.; van Baten, J. M. *Chem. Phys. Lett.* **2006**, *420*, 545–549.

(75) Vlugt, T. J. H.; Zhu, W.; Kapteijn, F.; Moulijn, J. A.; Smit, B.; Krishna, R. *J. Am. Chem. Soc.* **1998**, *120*, 5599–5600.

(76) Ban, S.; van Laak, A.; de Jongh, P. E.; van der Eerden, J. P. J. M.; Vlugt, T. J. H. *J. Phys. Chem. C* **2007**, *111*, 17241–17248.

(77) Krishna, R.; van Baten, J. M. *Sep. Purif. Technol.* **2007**, *55*, 246–255.

(78) Krishna, R.; van Baten, J. M. *Chem. Eng. J.* **2008**, *140*, 614–620.

(79) Murthi, M.; Snurr, R. Q. *Langmuir* **2004**, *20*, 2489–2497.

(80) Gupta, A.; Clark, L. A.; Snurr, R. Q. *Langmuir* **2000**, *16*, 3910–3919.

(81) Chmelik, C.; Heinke, L.; Kärger, J.; Shah, D. B.; Schmidt, W.; van Baten, J. M.; Krishna, R. *Chem. Phys. Lett.* **2008**, *459*, 141–145.

(82) Paschek, D.; Krishna, R. *Chem. Phys. Lett.* **2001**, *342*, 148–154.

(83) Krishna, R.; Paschek, D. *Chem. Eng. J.* **2002**, *85*, 7–15.

(84) Shah, D. B.; Guo, C. J.; Hayhurst, D. T. *J. Chem. Soc., Faraday Trans.* **1995**, *91*, 1143–1146.

(85) Krishna, R.; Vlugt, T. J. H.; Smit, B. *Chem. Eng. Sci.* **1999**, *54*, 1751–1757.

(86) Smit, B.; Maesen, T. L. M. *Nature* **1995**, *374*, 42–44.

(87) Floquet, N.; Simon, J. M.; Coulomb, J. P.; Bellat, J. P.; Weber, G.; Andre, G. *Microporous Mesoporous Mater.* **2009**, *122*, 61–71.

(88) Jobic, H.; Laloué, C.; Laroche, C.; van Baten, J. M.; Krishna, R. *J. Phys. Chem. B* **2006**, *110*, 2195–2201.

(89) Krishna, R.; Paschek, D.; Baur, R. *Microporous Mesoporous Mater.* **2004**, *76*, 233–246.

(90) Papadopoulos, G. K.; Jobic, H.; Theodorou, D. N. *J. Phys. Chem. B* **2004**, *108*, 12748–12756.

(91) Krishna, R.; van Baten, J. M.; García-Pérez, E.; Calero, S. *Ind. Eng. Chem. Res.* **2007**, *46*, 2974–2986.

(92) Krishna, R.; Li, S.; van Baten, J. M.; Falconer, J. L.; Noble, R. D. *Sep. Purif. Technol.* **2008**, *60*, 230–236.

(93) Krishna, R.; van Baten, J. M. *Microporous Mesoporous Mater.* **2009**, *125*, 126–134.

(94) Heinke, L.; Tzoulaki, D.; Chmelik, C.; Hibbe, F.; van Baten, J. M.; Lim, H.; Li, J.; Krishna, R.; Kärger, J. *Phys. Rev. Lett.* **2009**, *102*, 065901.

(95) Tzoulaki, D.; Heinke, L.; Lim, H.; Li, J.; Olson, D.; Caro, J.; Krishna, R.; Chmelik, C.; Kärger, J. *Angew. Chem., Int. Ed.* **2009**, *48*, 3525–3528.

(96) Krishna, R.; van Baten, J. M. *Chem. Eng. Technol.* **2007**, *30*, 1235–1241.

(97) Runnebaum, R. C.; Maginn, E. J. *J. Phys. Chem. B* **1997**, *101*, 6394–6408.

(98) Yoo, K.; Tsekov, R.; Smirniotis, P. G. *J. Phys. Chem. B* **2003**, *107*, 13593–13596.

(99) Gorring, R. L. *J. Catal.* **1973**, *31*, 13–26.

(100) Dubbeldam, D.; Calero, S.; Maesen, T. L. M.; Smit, B. *Angew. Chem., Int. Ed.* **2003**, *42*, 3624–3626.

(101) Dubbeldam, D.; Calero, S.; Maesen, T. L. M.; Smit, B. *Phys. Rev. Lett.* **2003**, *90* (24), 245901.

(102) Dubbeldam, D.; Smit, B. *J. Phys. Chem. B* **2003**, *107*, 12138–12152.

(103) Talu, O.; Sun, M. S.; Shah, D. B. *AIChE J.* **1998**, *44*, 681–694.

(104) Krishna, R.; van Baten, J. M. *Mol. Simul.* [Online early access]. http://dx.doi.org/10.1080/08927020902744672, **2009**.

(105) Ruthven, D. M. *Microporous Mesoporous Mater.* **2006**, *96*, 262–269.

(106) Jobic, H.; Methivier, A.; Ehlers, G.; Farago, B.; Haeussler, W. *Angew. Chem., Int. Ed.* **2004**, *43*, 364–366.

(107) Denayer, J. F. M.; Devriese, L. I.; Couck, S.; Martens, J. A.; Singh, R.; Webley, P. A.; Baron, G. V. *J. Phys. Chem. C* **2007**, *112*, 16593–16599.

(108) Daems, I.; Singh, R.; Baron, G. V.; Denayer, J. F. M. *Chem. Commun.* **2007**, 1316–1318.

(109) Dubbeldam, D.; Calero, S.; Vlugt, T. J. H.; Krishna, R.; Maesen, T. L. M.; Smit, B. *J. Phys. Chem. B* **2004**, *108*, 12301–12313.

(110) Calero, S.; Dubbeldam, D.; Krishna, R.; Smit, B.; Vlugt, T. J. H.; Denayer, J. F. M.; Martens, J. A.; Maesen, T. L. M. *J. Am. Chem. Soc.* **2004**, *126*, 11377–11386.

(111) Calero, S.; Lobato, M. D.; García-Pérez, E.; Mejías, J. A.; Lago, S.; Vlugt, T. J. H.; Maesen, T. L. M.; Smit, B.; Dubbeldam, D. *J. Phys. Chem. B* **2006**, *110*, 5838–5841.

(112) Demontis, P.; Jobic, H.; Gonzalez, M. A.; Suffritti, G. B. *J. Phys. Chem. C* **2009**, *113*, 12373–12379.

(113) Leroy, F.; Jobic, H. *Chem. Phys. Lett.* **2005**, *406*, 375–380.

(114) Pluth, J. J.; Smith, J. V. *J. Am. Chem. Soc.* **1980**, *102*, 4704–4708.

(115) Hedin, N.; DeMartin, G. J.; Strohmaier, K. G.; Reyes, S. C. *Microporous Mesoporous Mater.* **2007**, *98*, 182–188.

(116) Fritzsche, S.; Haberlandt, R.; Kärger, J.; Pfeifer, H.; Heinzinger, K.; Wolfsberg, M. *Chem. Phys. Lett.* **1995**, *242*, 361–366.

(117) Dubbeldam, D.; Beerdsen, E.; Calero, S.; Smit, B. *J. Phys. Chem. B* **2006**, *110*, 3164–3172.

(118) Plant, D. F.; Maurin, G.; Bell, R. G. *J. Phys. Chem. B* **2006**, *110*, 15926–15931.
(119) Koriabkina, A. O.; de Jong, A. M.; Schuring, D.; van Grondelle, J.; van Santen, R. A. *J. Phys. Chem. B* **2002**, *106*, 9559–9566.
(120) Millot, B.; Methivier, A.; Jobic, H.; Moueddeb, H.; Bee, M. *J. Phys. Chem. B* **1999**, *103*, 1096–1101.
(121) Millot, B.; Methivier, A.; Jobic, H.; Moueddeb, H.; Dalmon, J. A. *Microporous Mesoporous Mat.* **2000**, *38*, 85–95.
(122) Lee, Y.; Hriljac, J. A.; Vogt, T.; Parise, J. B.; Edmondson, M. J.; Anderson, P. A.; Corbin, D. R.; Nagai, T. *J. Am. Chem. Soc.* **2001**, *123*, 8418–8419.
(123) Combariza, A. F.; Sastre, G.; Corma, A. *J. Phys. Chem. C* **2009**, *113*, 11246–11253.
(124) Horcajada, P.; Serre, C.; Maurin, G.; Ramsahye, N. A.; Balas, F.; Vallet-Regí, M.; Sebban, M.; Taulelle, F.; Férey, G. *J. Am. Chem. Soc.* **2008**, *130*, 6774–6780.
(125) Ford, D. C.; Dubbeldam, D.; Snurr, R. Q. Diffusion Fundamentals 2009, to be published.
(126) Seehamart, K.; Nanok, T.; Krishna, R.; van Baten, J. M.; Remsungnen, T.; Fritzsche, S. *Microporous Mesoporous Mater.* **2009**, *125*, 97–100.
(127) Shindo, Y.; Hakuta, T.; Yoshitome, H.; Inoue, H. *J. Chem. Eng. Jpn.* **1983**, *16*, 120–126.
(128) Papadopoulos, G. K.; Nicholson, D.; Suh, S. H. *Mol. Simul.* **1999**, *22*, 237–256.
(129) Bae, J. S.; Do, D. D. *J. Non-Equilib. Thermodyn.* **2005**, *30*, 1–20.
(130) Bhatia, S. K.; Nicholson, D. *AIChE J.* **2006**, *52*, 29–38.
(131) Lund, L. M.; Berman, A. S. *J. Chem. Phys.* **1958**, *28*, 363–364.
(132) Hoang, V. T.; Huang, Q.; Eić, M.; Do, T. O.; Kaliaguine, S. *Langmuir* **2005**, *21*, 2051–2057.
(133) Gobin, O. C.; Huang, Q.; Hoang, V. T.; Kleitz, F.; Eić, M.; Kaliaguine, S. *J. Phys. Chem. C* **2007**, *111*, 3059–3065.
(134) Bhatia, S. K.; Nicholson, D. *J. Chem. Phys.* **2003**, *119*, 1719–1730.
(135) Krishna, R.; van Baten, J. M. *Chem. Eng. Sci.* **2009**, *64*, 870–882.
(136) Ruthven, D. M.; DeSisto, W.; Higgins, S. *Chem. Eng. Sci.* **2009**, *64*, 3201–3203.
(137) Higgins, S.; DeSisto, W.; Ruthven, D. M. *Microporous Mesoporous Mater.* **2009**, *117*, 268–277.
(138) Valiullin, R.; Kärger, J.; Gläser, R. *Phys. Chem. Chem. Phys.* **2009**, *11*, 2833–2853.
(139) Jakobtorweihen, S.; Lowe, C. P.; Keil, F. J.; Smit, B. *J. Chem. Phys.* **2007**, *127*, 024904.
(140) Maxwell, J. C. *Philos. Trans. R. Soc.* **1866**, *157*, 49–88.
(141) Stefan, J. *Sitzber. Akad. Wiss. Wien.* **1871**, *63*, 63–124.
(142) Lightfoot, E. N. *Transport phenomena and living systems*; John Wiley: New York, 1974.
(143) Young, J. B.; Todd, B. *Int. J. Heat Mass Transfer* **2005**, *48*, 5338–5353.
(144) Kerkhof, P. J. A. M. *Chem. Eng. J.* **1996**, *64*, 319–343.
(145) Mason, E. A.; Malinauskas, A. P. *Gas Transport in Porous Media: The Dusty-Gas Model*; Elsevier: Amsterdam, 1983.
(146) Krishna, R.; van Baten, J. M. *Ind. Eng. Chem. Res.* **2005**, *44*, 6939–6947.
(147) Poling, B. E.; Prausnitz, J. M.; O'Connell, J. P. *The Properties of Gases and Liquids*, 5th ed.; McGraw-Hill: New York, 2001.
(148) Kapteijn, F.; Moulijn, J. A.; Krishna, R. *Chem. Eng. Sci.* **2000**, *55*, 2923–2930.
(149) Skoulidas, A. I.; Sholl, D. S.; Krishna, R. *Langmuir* **2003**, *19*, 7977–7988.
(150) Krishna, R.; van Baten, J. M. *J. Phys. Chem. B* **2005**, *109*, 6386–6396.
(151) Sanborn, M. J.; Snurr, R. Q. *Sep. Purif. Technol.* **2000**, *20*, 1–13.
(152) Krishna, R.; Paschek, D. *Phys. Chem. Chem. Phys.* **2002**, *4*, 1891–1898.
(153) Jobic, H.; Kärger, J.; Bée, M. *Phys. Rev. Lett.* **1999**, *82*, 4260–4263.
(154) Krishna, R.; van Baten, J. M. *Ind. Eng. Chem. Res.* **2006**, *45*, 2084–2093.
(155) Lee, J. Y.; Olson, D. H.; Pan, L.; Emge, T. J.; Li, J. *Adv. Funct. Mater.* **2007**, *17*, 1255–1262.
(156) Vignes, A. *Ind. Eng. Chem. Fundamentals* **1966**, *5*, 189–199.
(157) Habgood, H. W. *Can. J. Chem.* **1958**, *36*, 1384–1397.
(158) Krishna, R.; van Baten, J. M. *Sep. Purif. Technol.* **2008**, *61*, 414–423.
(159) Krishna, R.; van Baten, J. M. *Chem. Phys. Lett.* **2007**, *446*, 344–349.
(160) Yu, M.; Falconer, J. L.; Noble, R. D.; Krishna, R. *J. Membr. Sci.* **2007**, *293*, 167–173.
(161) Liu, B.; Smit, B. *Langmuir* **2009**, *25*, 5918–5926.
(162) Babarao, R.; Jiang, J.; Sandler, S. I. *Langmuir* **2009**, *25*, 5239–5247.
(163) van de Graaf, J. M.; Kapteijn, F.; Moulijn, J. A. *AIChE J.* **1999**, *45*, 497–511.
(164) Bakker, W. J. W. Structured systems in gas separation. Ph.D. Thesis, Delft University of Technology, Delft, The Netherlands, 1999.
(165) Krishna, R.; Paschek, D. *Sep. Purif. Technol.* **2000**, *21*, 111–136.
(166) Vroon, Z. A. E. P.; Keizer, K.; Gilde, M. J.; Verweij, H.; Burggraaf, A. J. *J. Membr. Sci.* **1996**, *113*, 293–300.
(167) Dong, J.; Lin, Y. S.; Liu, W. *AIChE J.* **2000**, *46*, 1957–1966.
(168) Smit, B.; Krishna, R. *Chem. Eng. Sci.* **2003**, *58*, 557–568.
(169) Pera-Titus, M.; Llorens, J.; Tejero, J.; Cunill, F. *Catal. Today* **2006**, *118*, 73–84.
(170) Pera-Titus, M.; Fité, C.; Sebastián, V.; Lorente, E.; Llorens, J.; Cunill, F. *Ind. Eng. Chem. Res.* **2008**, *47*, 3213–3224.
(171) Fernandez, M.; Kärger, J.; Freude, D.; Pampel, A.; van Baten, J. M.; Krishna, R. *Microporous Mesoporous Mater.* **2007**, *105*, 124–131.
(172) Chmelik, C.; Heinke, L.; van Baten, J. M.; Krishna, R. *Microporous Mesoporous Mater.* **2009**, *125*, 11–16.
(173) Jiang, M.; Eic, M.; Miachon, S.; Dalmon, J. A.; Kocirik, M. *Sep. Purif. Technol.* **2001**, *25*, 287–295.
(174) Förste, C.; Germanus, A.; Kärger, J.; Pfeifer, H.; Caro, J.; Pilz, W.; Zikánová, A. *J. Chem. Soc., Faraday Trans. 1* **1987**, *83*, 2301–2309.
(175) Gupta, A.; Snurr, R. Q. *J. Phys. Chem. B* **2005**, *109*, 1822–1833.
(176) Schuring, D.; Koriabkina, A. O.; de Jong, A. M.; Smit, B.; van Santen, R. A. *J. Phys. Chem. B* **2001**, *105*, 7690–7698.
(177) Namba, S.; Sato, K.; Fujita, K.; Kim, J. H.; Yashima, T. *Stud. Surf. Sci. Catal.* **1986**, *28*, 661–668.
(178) Santilli, D. S. *J. Catal.* **1986**, *99*, 335–341.
(179) Calero, S.; Smit, B.; Krishna, R. *J. Catal.* **2001**, *202*, 395–401.
(180) Calero, S.; Smit, B.; Krishna, R. *Phys. Chem. Chem. Phys.* **2001**, *3*, 4390–4398.
(181) Yu, M.; Falconer, J. L.; Noble, R. D. *Langmuir* **2005**, *21*, 7390–7397.
(182) Gump, C. J.; Noble, R. D.; Falconer, J. L. *Ind. Eng. Chem. Res.* **1999**, *38*, 2775–2781.
(183) Krishna, R.; Paschek, D. *Ind. Eng. Chem. Res.* **2000**, *39*, 2618–2622.
(184) Jolimaitre, E.; Ragil, K.; Tayakout-Fayolle, M.; Jallut, C. *AIChE J.* **2002**, *48*, 1927–1937.
(185) Krishna, R.; Baur, R. *Chem. Eng. Sci.* **2005**, *60*, 1155–1166.
(186) Baur, R.; Krishna, R. *Chem. Eng. J.* **2005**, *109*, 107–113.
(187) Aris, R. *The mathematical theory of diffusion and reaction in permeable catalysts*; Clarendon Press: Oxford, 1975.
(188) Baur, R.; Krishna, R. *Chem. Eng. J.* **2004**, *99*, 105–116.
(189) Baur, R.; Krishna, R. *Catal. Today* **2005**, *105*, 173–179.
(190) Hansen, N.; Krishna, R.; van Baten, J. M.; Bell, A. T.; Keil, F. J. *J. Phys. Chem. C* **2009**, *113*, 235–246.
(191) Keffer, D.; Gupta, V.; Kim, D.; Lenz, E.; Davis, H. T.; McCormick, A. V. *J. Mol. Graphics* **1996**, *14*, 108–116.
(192) Krishna, R.; van Baten, J. M. *Chem. Phys. Lett.* **2005**, *407*, 159–165.

JP906879D